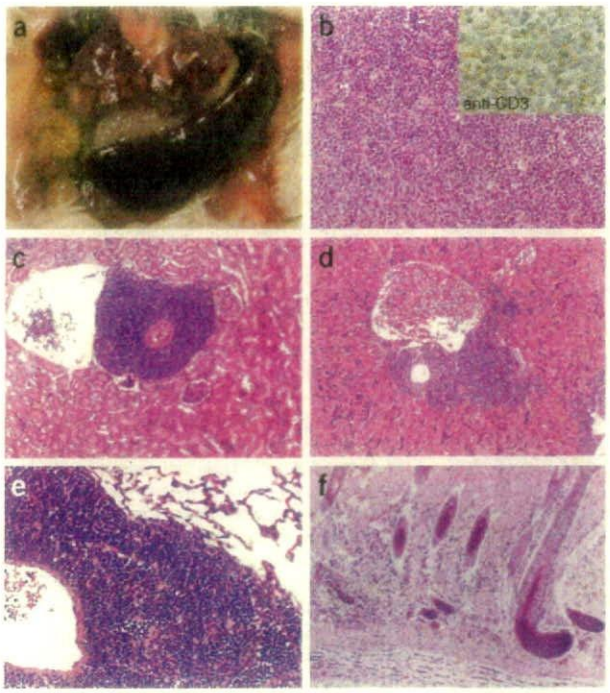

Figure 3 Gross and histological findings of lymphoma in SCID mice at 28 d after intradermal injection of lymphomatous cells from Tax transgenic mice. (**a**) Gross splenomegaly. Histological findings in spleen (**b**; insert, immunostaining showing positive staining for CD3-specific antibody), liver (**c**), kidney (**d**), lung (**e**) and skin (**f**). All organs showed extensive lymphomatous invasion.

direct transfer of cells from three transgenic mice, all SCID mice died within 28 d, having developed both an extremely aggressive leukemia with characteristic flower cells (**Fig. 2m**) and extensive lymphomatous involvement of the spleen, lymph nodes, bone marrow, liver, kidney and lung, which was identical to that observed in the original transgenic mice (**Fig. 3**). Notably, cutaneous involvement was only observed in those mice into which cells had been transferred by intradermal injection. Transmission electron microscopy of leukemic cells recovered from ascites fluid from SCID mice showed grossly enlarged and segmented cerebriform nuclei with markedly thin and scanty cytoplasms and a loss of polarity similar to that reported for ATLL and Sezary syndrome (**Fig. 2o**).

Flow cytometry analysis

We used flow cytometry to characterize the cell populations in both transgenic and SCID mice. Cells from transgenic spleens showed marked size heterogeneity with considerably higher forward scatter and side scatter compared to cells derived from spleens of control mice (**Fig. 4a**). Immunostaining of cells from SCID mice showed these were a distinct population and had a $CD3^-CD4^-CD8^-CD34^-c\text{-}kit^-$ phenotype (**Fig. 4b,c**). Staining for B-cell markers (B220) and macrophage markers (Mac 1) was negative (data not shown). Further analysis of SCID mice showed that the cells were $CD44^+CD25^+$ (**Fig. 4c**) and positive for cytoplasmic but not surface CD3 in both flow cytometric and immunofluorescence studies (**Fig. 4d,e**), all of which is consistent with a pre–T-cell, double-negative phenotype (**Fig. 4f**). A characteristic feature of ATLL is overexpression of CD25 (also known as IL-2 receptor α) on the surface of the transformed cells, and it is believed that Tax-mediated upregulation of both interleukin (IL)-2 and the IL-2 receptor has a major role in the autonomous proliferation of the transformed cell populations[14]. We examined the expression of CD25 in splenic lymphoma cells, and although the expression levels varied between tumor cells from different mice, a marked increase in expression was always evident (**Fig. 4d**). In addition, the T-cell activation marker CD69 was also found to be expressed at high levels on the lymphomatous cells (**Fig. 4d**).

NF-κB activation in transgenic and SCID mice

As it is well established that activation of NF-κB by Tax has a crucial role in transformation of cells by HTLV-I and in the maintenance of the malignant phenotype[12–14], we examined activity of NF-κB using both electrophoretic mobility shift assays (EMSAs) and enzyme-linked immunosorbent assays (ELISAs). EMSAs on nuclear extracts from transgenic splenic lymphoma cells showed marked NF-κB activity (**Fig. 5**) similar to that in a Epstein-Barr virus–transformed lymphoblastoid cell line used as a positive control. In contrast, no activity was evident in cells from normal mice (**Fig. 5a**). In addition, supershift assays (**Fig. 5b**) showed supershifted bands in the presence of antibodies for p50 and c-Rel, suggesting that formation of the p50–c-Rel complex is involved in the development and maintenance of the malignant phenotype (**Fig. 5b**). Evaluation of lymphomatous cells from SCID mice also confirmed activation of NF-κB. In contrast to the case of transgenic mice, this activation was found to involve only c-rel (**Supplementary Fig. 1** online). We also examined SCID mice by ELISA for activation of CREB, which was shown to be absent (**Supplementary Fig. 1** online).

Expression of Tax in transgenic mice

We used RT-PCR analysis of RNAs from splenic tissues to determine whether development of disease in both transgenic and SCID mice was associated with active expression of Tax (**Fig. 1c**). Although expression levels were low (10^4 less than expression of *Actb*, which encodes β-actin), Tax mRNA could be readily detected in newborn, asymptomatic, early-killed mice and in both transgenic and SCID mice with overt disease.

DISCUSSION

Here we showed that Tax expression alone in transgenic mice is sufficient to initiate the development of T-cell lymphoma and leukemia with clinical, pathological and immunological features similar or identical to those observed in ATLL. Specifically, the disorder in mice occurs after prolonged latency periods ranging from 10 to 23 months, which would be equivalent to the 20–60 years observed in human disease. The long time period before the onset of disease in the transgenic mouse model is also consistent with a multistep process of transformation. The clinical and pathological features of the disease were identical to those observed in the aggressive forms of ATLL, with widespread organ invasion by lymphomatous cells and the development of leukemia. Notably, the leukemia displayed the typical appearance of flower cells characteristic of ATLL, and these cells also had the expected morphological features when examined by electron microscopy.

ATLL has prominent cutaneous involvement, and this was reproduced in the transgenic model. Transgenic mice were also clinically immunocompromised and developed pulmonary infections with *P. jiroveci*, which is also characteristic of ATLL. The development of disease in transgenic mice and after transfer of disease to SCID mice was associated with activation of NF-κB, which is also found in ATLL.

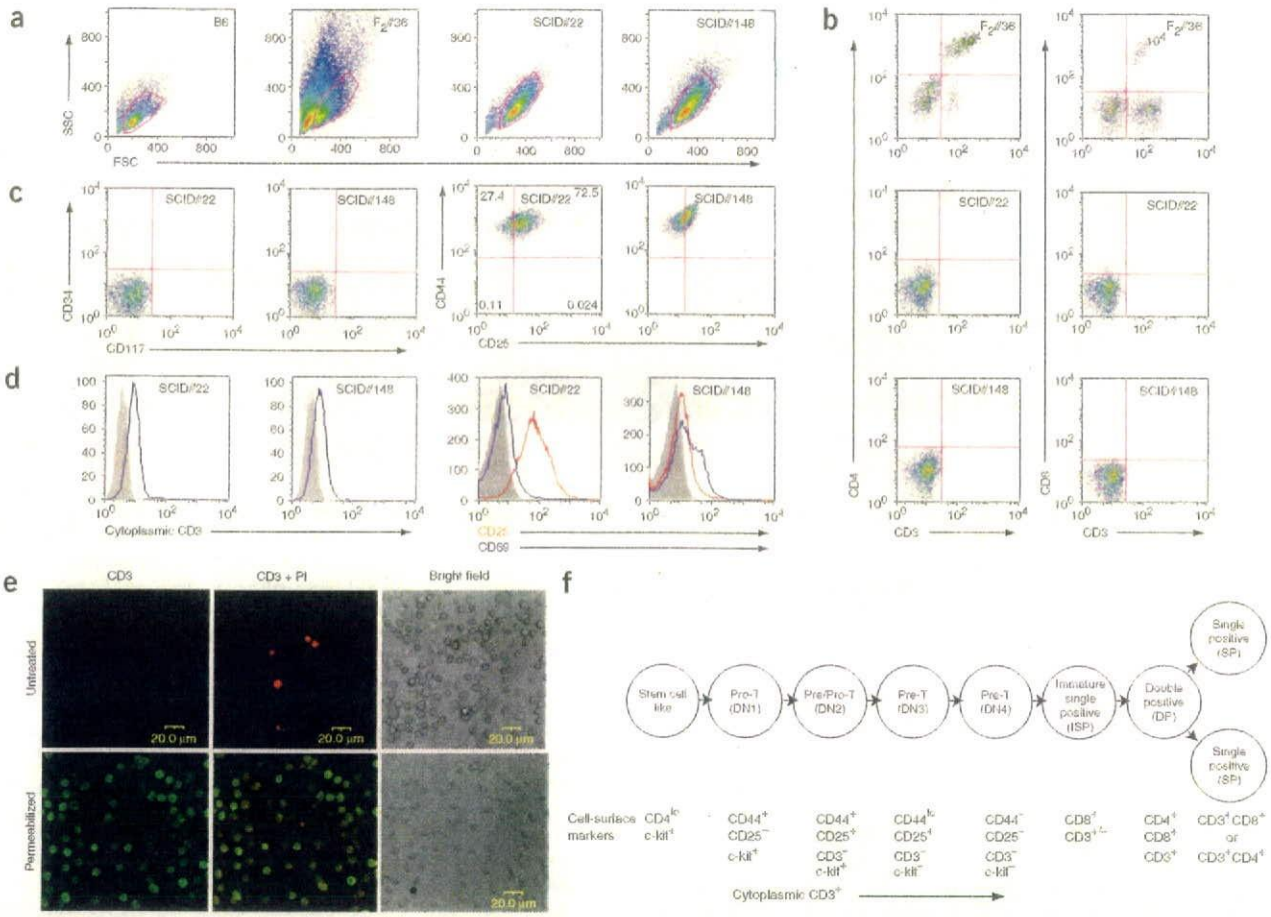

Figure 4 Flow cytometry analysis of cell-surface and intracellular markers in lymphomatous cells. We analyzed spleen-cell suspensions from transgenic mice with leukemia-lymphoma (#36), littermate control mouse (B6) and two SCID mice (#22, #148) with overt disease. (**a**) Forward-scatter (FSC) and side-scatter (SSC) analysis. (**b**) Expression of cell-surface markers CD3, CD4 and CD8. (**c**) Expression of cell-surface markers CD34, CD117 (also known as c-kit), CD44 and CD25. (**d**) Expression of CD25, CD69 and cytoplasmic CD3. (**e**) Surface and cytoplasmic CD3 staining of lymphomatous cells from SCID mice (SCID #22) with fulminant disease. Immunofluorescence studies show an absence of CD3 surface staining (untreated) but consistent and uniform cytoplasmic staining in permeabilized cells. Staining of nuclei using propidium iodide (PI) is indicated. (**f**) Schematic representation of T-cell development and corresponding immunological markers in the mouse thymus.

In the transgenic mice, this involved both the p50 and c-rel components, whereas after transfer to SCID mice, only c-rel seemed to be involved. The reasons for this are unclear, but such differences have also been observed in individuals with ATLL[24].

The malignant phenotype observed in the transgenic mice was a $CD4^-CD8^-$ double negative. Flow cytometric analysis also showed that transformed cells were $CD44^+$ and c-kit^-. Although surface staining for CD3 was negative, cytoplasmic CD3 staining was readily shown, and overall the cell markers were consistent with a thymic pre–T-cell phenotype[25,26]. The most common presenting phenotype in ATLL is $CD4^+$; however, there have been numerous reports describing the $CD4^-CD8^-$ phenotype in a considerable number of individuals with ATLL[3–7]. The different phenotypes observed in ATLL may well reflect the temporal relationships between infection with expression of Tax and the cell populations present at different stages of thymic development. It is likely that infection in most cases of human disease occurs after birth and much later than in our model. We are currently exploring the possibility of modifying the Lck promoters to allow control of Tax expression at different stages of thymic development to assess whether this will result in different phenotypes. It seems highly probable that use of the Lck promoter, which restricts expression of the transgene to developing thymocytes, has been crucial to the success of our mouse model. As noted previously, ATLL occurs after vertical transmission and is specifically associated with a history of breastfeeding. In rat models, intravenous or intraperitoneal inoculation of HTLV-I–infected cell lines results in considerable humoral and cellular immune responses. In contrast, these are absent after oral inoculation, and this hyporesponsiveness seems to contribute to successful infection[27]. Thus, both oral tolerance and the tropism of the virus for infection of developing T lymphocytes seem to be two key factors in the development of ATLL.

One major difference between our model and human disease is expression of Tax. Expression of Tax is rarely detected in ATLL, and this circumstance is thought to result primarily from highly efficient Tax-specific cellular immune responses that can effectively eliminate Tax-expressing T lymphocytes. Such responses, however, would certainly not occur in either transgenic or SCID mice. It has also been suggested that the lack of Tax expression in ATLL may be the result of

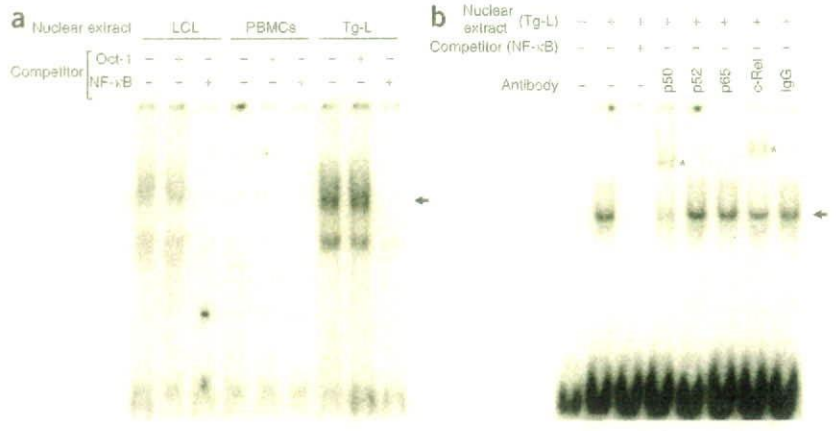

Figure 5 EMSAs showing activation of NF-κB in lymphomatous cells. (**a**) EMSAs of nuclear extracts from lymphomatous cells of transgenic mice and a positive control, the Epstein-Barr virus–transformed lymphoid cell line, and normal mouse PBMCs with a radiolabled NF-κB binding oligonucleotide probe. Specific shifted bands of NF-κB binding proteins (arrow) were exclusively detected in nuclear extracts from lymphoblastoid cell line and transgenic mice with disease (Tg-L) in the presence of the competitor. (**b**) Supershift assay of nuclear extracts from Tg-L using antibodies against p50, p65, p52, and c-Rel. Normal IgG was used as control. Supershifted bands were detected in extracts with p50-specific and c-Rel–specific antibodies.

epigenetic changes that restrict viral gene expression, but it is presently unclear whether such changes might at some point develop in this transgenic mouse model.

The models of ATLL developed in both transgenic and SCID mice will now allow detailed investigation of the role of Tax and the identification of specific molecular events associated with transformation. Moreover, the rapid development of fulminant disease in SCID mice will uniquely facilitate the evaluation of a range of therapeutic interventions that may ultimately lead to more effective treatments of human disease.

METHODS

Details are in **Supplementary Methods** online.

Mice. All mouse experimental protocols were approved by the Animal Care and Use Committee of the National Institute of Infectious Diseases, Tokyo, Japan, and by the Animal Research Ethics Committee of University College Dublin, Ireland. We purchased C57BL/6 mice from Charles River and the Oriental Yeast Company. We obtained SCID mice from Clea Japan.

Plasmid construction and generation of transgenic mice. We generated transgenic mice using inbred C57BL/6 mice and standard methods. We prepared the transgene construct (p*Lck*-Tax) by subcloning the HTLV-I Tax coding sequence into the *Bam*HI site of p1017 (provided by R.M. Perlmutter, University of Washington). We amplified Tax cDNA by PCR from DNA extracted from infected peripheral blood mononuclear cells (PBMCs). The p*Lck*-Tax plasmid was linearized by digestion with *Not*I (Boerhinger Mannheim), resulting in a 6.3-kb fragment containing the transgene, and this was purified using a Qiaex gel extraction kit (Qiagen) before injection. All mice were housed under specific pathogen-free conditions. Mice were killed after anesthesia with chloroform by syringe cardiac exsanguination. For detection of the transgene, we performed Southern blotting on genomic DNA extracted from tail-tip biopsies.

Chromosomal mapping of the inserted transgene. We identified genomic sequences flanking the transgenes by genomic walking methods[28] using the Universal Genome Walker kit (BD Bioscience Clontech) according to the manufacturer's instructions. Briefly, we constructed adaptor-ligated genomic DNA libraries of the transgenic mice using tail-tip DNA digested with four restriction enzymes: *Dra*I, *Pvu*II, *Eco*RV and *Stu*I; the genomic walk consisted of two PCR amplifications. We determined nucleotide sequences of PCR products by direct sequencing and identified specific chromosomal transgene insertion sites using BLAST searches of the flanking sequences in the Ensembl genome database.

Histopathological examination and immunohistochemistry. We directly fixed tissues in neutral-buffered formalin (Sigma), embedded them in paraffin, and sectioned and stained them with H&E. We stained additional sections with Grocott staining for detection of *P. jiroveci* cysts. We stained skin sections with CD3-specific antibody (Santa Cruz Biotechnology). We prepared peripheral blood smears using Giemsa staining and examined them with light microscopy.

Flow cytometry. We performed flow cytometry with a FACSCalibur (BD Bioscience Clontech) using standard methods. Briefly, we prepared single-cell suspensions from spleen in PBS containing 2% FCS and 0.05% sodium azide. For detection of surface antigens, we washed cells and stained them with saturating amounts of antibodies conjugated with FITC, PE or APC in the presence of blocking antibody 2.4G2 (FcR-specific) monoclonal antibody for 20 min on ice. For analysis of live cells, we added propidium iodide at a final concentration of 5 μg/ml. For detection of intracellular CD3, we stained cells with ethidium monoazide bromide (5 μg/ml), fixed them with 4% formaldehyde in PBS and incubated them in permeabilization buffer containing 0.5% saponin. We incubated cells with FITC-conjugated CD3-specific antibody or control monoclonal antibody (rat IgG2b). We carried out analysis using the Cell Quest program and reanalyzed data using FlowJo software (Tree Star) by gating live cells. Specific monoclonal antibodies used are detailed in **Supplementary Methods** online.

Immunofluorescence studies of surface and cytoplasmic CD3 staining. We collected cells (10^6) directly from spleen tissues from SCID mice, and washed and incubated them with CD3-specific antibody. Thereafter, we incubated samples with Alexa 488R–conjugated goat rabbit-specific IgG and then stained with propidium iodide (1 μg/ml). We permeabilized cells before incubation with primary antibody and detected immunofluorescent signals using a confocal microscope (IX70, Olympus).

EMSAs. We prepared nuclear extracts from 1–10 × 10^6 of lymphomatous cells from spleens of transgenic mice, an Epstein-Barr virus–transformed lymphoblastoid cell line, and PBMCs from control mice as previously described[29]. We performed an EMSA with the Gel Shift Assay Systems kit (Promega) according to the manufacturer's protocol. We separated samples by electrophoresis on 4% polyacrylamide gels in 0.25% Tris–boric acid–EDTA, and dried and analyzed them using a BAS 2000 image analyzer (Fujifilm).

Real-time quantitative PCR. We used real-time PCR (RT-PCR) to quantify expression of Tax mRNA in transgenic and SCID mice. We harvested spleens at birth and at 8 weeks, 11 weeks, 5 months, 18 months in transgenic mice without disease, and at 18 months in mice with leukemia-lymphoma, from control littermates and from SCID mice after intraperitoneal transfer of lymphomatous cells. We measured levels of Tax mRNA by RT-PCR after reverse transcription using the ABI PRISM 7900 sequence detection system (Applied Biosystems) with a QuantiTect Probe PCR kit (Qiagen).

Transfer of leukemia and lymphoma to SCID mice. We harvested spleen cells from transgenic mice and directly suspended them in RPMI medium. We directly injected cells (10^6) intraperitoneally or intradermally into SCID mice

from three individual transgenic animals. At 28 d, when mice were clearly ill, we carried out pathological and immunological studies as above.

Electron microscopy. We collected cells from ascites of SCID mice and fixed them in 2.5% glutaraldehye and 2% paraformaldehyde, postfixed them in 1% osmium tetroxide, dehydrated them and embedded them in epoxy resin. We stained ultrathin, 80-nm sections with uranyl and lead acetate and examined them with a JEM-1220 electron microscope (Jeol Datum) at 80 kV.

URL. Ensembl, http://www.ensembl.org

Note: Supplementary information is available on the Nature Medicine website.

ACKNOWLEDGMENTS

We thank Y. Sato and E. Tao for their technical assistance. We also thank O. Suzuki, T. Suzuki, M. Moriyama, K. Iwabuchi and Y. Misaki for advice. Y.O. is a Research Fellow of the Japanese Society for the Promotion of Science. These studies were supported by the Japanese Foundation for AIDS Prevention, Core Research for Evolutional Science and Technology (CREST), Ministry of Education and Culture, Japan and the National Virus Reference Laboratory, University College Dublin, Ireland.

COMPETING INTERESTS STATEMENT

The authors declare that they have no competing financial interests.

Published online at http://www.nature.com/naturemedicine/
Reprints and permissions information is available online at http://npg.nature.com/reprintsandpermissions/

1. Matsuoka, M. Human T-cell leukemia virus type I and adult T-cell leukemia. *Oncogene* **22**, 5131–5140 (2003).
2. Takatsuki, K. *et al.* Clinical diversity in adult T-cell leukemia-lymphoma. *Cancer Res.* **45**, 4644s–4645s (1985).
3. Hattori, T. *et al.* Leukaemia of novel gastrointestinal T-lymphocyte population infected with HTLV-I. *Lancet* **337**, 76–77 (1991).
4. Suzushima, H. *et al.* Double-negative (CD4- CD8-) T cells from adult T-cell leukemia patients also have poor expression of the T-cell receptor alpha beta/CD3 complex. *Blood* **81**, 1032–1039 (1993).
5. Kamihira, S. *et al.* Unusual morphological features of adult T-cell leukemia cells with aberrant immunophenotype. *Leuk. Lymphoma* **12**, 123–130 (1993).
6. Suzushima, H., Asou, N., Hattori, T. & Takatsuki, K. Adult T-cell leukemia derived from S100 beta positive double-negative (CD4- CD8-) T cells. *Leuk. Lymphoma* **13**, 257–262 (1994).
7. Shimauchi, T., Hirokawa, Y. & Tokura, Y. Purpuric adult T-cell leukaemia/lymphoma: expansion of unusual CD4/CD8 double-negative malignant T cells expressing CCR4 but bearing the cytotoxic molecule granzyme B. *Br. J. Dermatol.* **152**, 350–352 (2005).
8. Yamada, Y. *et al.* Adult T-cell leukemia with atypical surface phenotypes: clinical correlation. *J. Clin. Oncol.* **3**, 782–788 (1985).
9. Ohata, J. *et al.* CD4/CD8 double-positive adult T-cell leukemia with preceding cytomegaloviral gastroenterocolitis. *Int. J. Hematol.* **69**, 92–95 (1999).
10. Ciminale, V. *et al.* Unusual CD4+CD8+ phenotype in a Greek patient diagnosed with adult T-cell leukemia positive for human T-cell leukemia virus type I (HTLV-I). *Leuk. Res.* **24**, 353–358 (2000).
11. Uchiyama, T., Yodoi, J., Sagawa, K., Takatsuki, K. & Uchino, H. Adult T-cell leukemia: clinical and hematologic features of 16 cases. *Blood* **50**, 481–492 (1977).
12. Yoshida, M. Multiple viral strategies of HTLV-1 for dysregulation of cell growth control. *Annu. Rev. Immunol.* **19**, 475–496 (2001).
13. Jeang, K.T., Giam, C.Z., Majone, F. & Aboud, M. Life, death, and tax: role of HTLV-I oncoprotein in genetic instability and cellular transformation. *J. Biol. Chem.* **279**, 31991–31994 (2004).
14. Sun, S.C. & Yamaoka, S. Activation of NF-kappaB by HTLV-I and implications for cell transformation. *Oncogene* **24**, 5952–5964 (2005).
15. Hall, W.W. & Fujisawa, M. Deregulation of cell-signalling pathways in HTLV-I infection. *Oncogene* **24**, 5965–5975 (2005).
16. Nerenberg, M., Hinrichs, S.H., Reynolds, R.K., Khoury, G. & Jay, G. The tat gene of human T-lymphotropic virus type 1 induces mesenchymal tumors in transgenic mice. *Science* **237**, 1324–1329 (1987).
17. Hinrichs, S.H., Nerenberg, M., Reynolds, R.K., Khoury, G. & Jay, G. A transgenic mouse model for human neurofibromatosis. *Science* **237**, 1340–1343 (1987).
18. Green, J.E., Hinrichs, S.H., Vogel, J. & Jay, G. Exocrinopathy resembling Sjogren's syndrome in HTLV-1 tax transgenic mice. *Nature* **341**, 72–74 (1989).
19. Iwakura, Y. *et al.* Induction of inflammatory arthropathy resembling rheumatoid arthritis in mice transgenic for HTLV-I. *Science* **253**, 1026–1028 (1991).
20. Green, J.E., Baird, A.M., Hinrichs, S.H., Klintworth, G.K. & Jay, G. Adrenal medullary tumors and iris proliferation in a transgenic mouse model of neurofibromatosis. *Am. J. Pathol.* **140**, 1401–1410 (1992).
21. Grossman, W.J. *et al.* Development of leukemia in mice transgenic for the tax gene of human T-cell leukemia virus type I. *Proc. Natl. Acad. Sci. USA* **92**, 1057–1061 (1995).
22. Chaffin, K.E. *et al.* Dissection of thymocyte signaling pathways by *in vivo* expression of pertussis toxin ADP-ribosyltransferase. *EMBO J.* **9**, 3821–3829 (1990).
23. Wildin, R.S. *et al.* Developmental regulation of lck gene expression in T lymphocytes. *J. Exp. Med.* **173**, 383–393 (1991).
24. Mori, N. *et al.* Constitutive activation of NF-kappaB in primary adult T-cell leukemia cells. *Blood* **93**, 2360–2368 (1999).
25. Staal, F.J., Weerkamp, F., Langerak, A.W., Hendriks, R.W. & Clevers, H.C. Transcriptional control of T lymphocyte differentiation. *Stem Cells* **19**, 165–179 (2001).
26. Rezuke, W.N., Abernathy, E.C. & Tsongalis, G.J. Molecular diagnosis of B- and T-cell lymphomas: fundamental principles and clinical applications. *Clin. Chem.* **43**, 1814–1823 (1997).
27. Kannagi, M., Ohashi, T., Harashima, N., Hanabuchi, S. & Hasegawa, A. Immunological risks of adult T-cell leukemia at primary HTLV-I infection. *Trends Microbiol.* **12**, 346–352 (2004).
28. Noguchi, A. *et al.* Chromosomal mapping and zygosity check of transgenes based on flanking genome sequences determined by genomic walking. *Exp. Anim.* **53**, 103–111 (2004).
29. Dignam, J.D., Martin, P.L., Shastry, B.S. & Roeder, R.G. Eukaryotic gene transcription with purified components. *Methods Enzymol.* **101**, 582–598 (1983).

Retrovirology

BioMed Central

Research

Open Access

SUV39H1 interacts with HTLV-1 Tax and abrogates Tax transactivation of HTLV-1 LTR

Koju Kamoi[1,2], Keiyu Yamamoto, Aya Misawa[1], Ariko Miyake[1], Takaomi Ishida[1], Yuetsu Tanaka[3], Manabu Mochizuki[2] and Toshiki Watanabe*[1]

Address: [1]Laboratory of Tumor Cell biology, Department of Medical Genome Sciences, Graduate School of Frontier Sciences, The University of Tokyo, 4-6-1 Shirokanedai, Minato-ku, Tokyo 108-8639, Japan, [2]Department of Ophthalmology and Visual Science, Graduate School, Tokyo Medical and Dental University, 1-5-45 Yushima, Bunkyo-ku, Tokyo 113-8519, Japan and [3]Department of Immunology, Graduate School of Medicine, University of the Ryukyus, Okinawa 903-0215, Japan

Email: Koju Kamoi - koju1030@ims.u-tokyo.ac.jp; Keiyu Yamamoto - keiyu@ims.u-tokyo.ac.jp; Aya Misawa - ayamsw@ims.u-tokyo.ac.jp; Ariko Miyake - amiyake@ims.u-tokyo.ac.jp; Takaomi Ishida - tishida@ims.u-tokyo.ac.jp; Yuetsu Tanaka - yuetsu@ma.kcom.ne.jp; Manabu Mochizuki - m.manabu.oph@tmd.ac.jp; Toshiki Watanabe* - tnabe@ims.u-tokyo.ac.jp

* Corresponding author

Published: 13 January 2006

Retrovirology 2006, **3**:5 doi:10.1186/1742-4690-3-5

Received: 11 November 2005
Accepted: 13 January 2006

This article is available from: http://www.retrovirology.com/content/3/1/5

Abstract

Background: Tax is the oncoprotein of HTLV-1 which deregulates signal transduction pathways, transcription of genes and cell cycle regulation of host cells. Transacting function of Tax is mainly mediated by its protein-protein interactions with host cellular factors. As to Tax-mediated regulation of gene expression of HTLV-1 and cellular genes, Tax was shown to regulate histone acetylation through its physical interaction with histone acetylases and deacetylases. However, functional interaction of Tax with histone methyltransferases (HMTase) has not been studied. Here we examined the ability of Tax to interact with a histone methyltransferase SUV39H1 that methylates histone H3 lysine 9 (H3K9) and represses transcription of genes, and studied the functional effects of the interaction on HTLV-1 gene expression.

Results: Tax was shown to interact with SUV39H1 *in vitro*, and the interaction is largely dependent on the C-terminal half of SUV39H1 containing the SET domain. Tax does not affect the methyltransferase activity of SUV39H1 but tethers SUV39H1 to a Tax containing complex in the nuclei. In reporter gene assays, co-expression of SUV39H1 represses Tax transactivation of HTLV-1 LTR promoter activity, which was dependent on the methyltransferase activity of SUV39H1. Furthermore, SUV39H1 expression is induced along with Tax in JPX9 cells. Chromatin immunoprecipitation (ChIP) analysis shows localization of SUV39H1 on the LTR after Tax induction, but not in the absence of Tax induction, in JPX9 transformants retaining HTLV-1-Luc plasmid. Immunoblotting shows higher levels of SUV39H1 expression in HTLV-1 transformed and latently infected cell lines.

Conclusion: Our study revealed for the first time the interaction between Tax and SUV39H1 and apparent tethering of SUV39H1 by Tax to the HTLV-1 LTR. It is speculated that Tax-mediated tethering of SUV39H1 to the LTR and induction of the repressive histone modification on the chromatin through H3 K9 methylation may be the basis for the dose-dependent repression of Tax transactivation of LTR by SUV39H1. Tax-induced SUV39H1 expression, Tax-SUV39H1 interaction and tethering to the LTR may provide a support for an idea that the above sequence of events may form a negative feedback loop that self-limits HTLV-1 viral gene expression in infected cells.

Background

Human T-cell leukemia virus type 1 (HTLV-1) is the causative agent of an aggressive leukemia known as adult T-cell leukemia (ATL), as well as HTLV-1 associated myelopathy/tropical spastic paraparesis (HAM/TSP) and HTLV-1 uveitis (HU). These diseases develop usually after more than 40 years of clinical latency [1-4]. No or little, if any, viral gene expression can be detected in the peripheral blood of HTLV-1 carriers or ATL cells, indicating that HTLV-1 is infected latently *in vivo* [5,6].

The viral protein Tax plays a central role in the development of diseases mentioned above in HTLV-1-infected carriers. Tax can activate transcription of the HTLV-1 genome as well as specific cellular genes including inflammatory cytokines and their receptors and adhesion molecules. Tax also shows transforming activity when expressed in T lymphocytes and fibroblasts [7-10]. Tax is a 40-kDa nuclear phosphoprotein which is translated from a spliced HTLV-1 mRNA transcribed from the 3' portion of the genome. Tax regulates multiple cellular responses by its protein-protein interactions with various host cellular factors. In the regulation of transcription, Tax does not bind DNA directly but stimulates transcription from the HTLV-1 LTR and from the promoters of specific cellular genes by recruiting cellular transcription factors. Tax-mediated transcriptional regulation is based on its interaction with DNA-binding transcription factors such as members of the cyclic AMP response element binding protein/activating transcription factor (CREB/ATF), the nuclear factor-κB (NF-κB), and the serum response factor (SRF) and with two related transcriptional co-activators CREB binding protein (CBP) and p300.

In order to activate transcription of the HTLV-1 genome, nuclear Tax interacts with the CREB/ATF family of transcriptional activators, which bind to the viral long terminal repeat (LTR) [11-14]. The interaction of Tax with CREB and the CREB response elements in the LTR results in a CREB response element-CREB-Tax ternary complex [10]. Tax also binds directly to the KIX domain of the transcriptional co-activators CREB-binding protein (CBP) and p300 [15,16]. CBP and p300 are histone acetylases and acetylate substrates such as histones and transcription factors and may serve as integrators of numerous cellular signaling processes with the basal RNA polymerase II machinery [17,18]. This would, in turn, allow controlled regulation and interaction with many cellular transcription factors including CREB, NF-κB/Rel, p53, c-Myb, c-Jun, c-Fos, and transcription factor IIB in a signal-dependent and, sometimes, mutually exclusive fashion. In this context, Tax-mediated repression of transcription of some cellular genes are explained by functional competition between transcription factors and Tax [19]. A recent report that Tax interacts with a histone deacetylase (HDAC) [20] showed a novel mechanism by which Tax represses transcription of certain target genes. HDAC1 is likely to compete with CBP in binding to Tax and functions as a negative regulator of the transcriptional activation by Tax.

Reversible modification of core histones plays an important role in the regulation of gene expression, such as acetylation, phosphorylation and methylation [21,22]. These covalent modifications, alone or in combination, act as a scaffold for the recruitment of specific regulatory proteins or protein complexes that participate in certain downstream nuclear process including transcription, replication and repair [23]. Thus, it is thought that this "histone code" may serve to establish and maintain distinct chromosomal domains that are epigenetically transmitted [24,25]. Consistent with the histone code, it has been revealed that the methylation of histone H3 lysine 9 (H3 K9), a modification associated with transcriptionally silent heterochromatin, is critical for long-range chromatin regulatory processes [26,27]. Several enzymes are known to methylate H3 K9, such as murine SUV39H1 and G9a proteins [28,29].

Although regulation of histone acetylation by Tax through its physical interaction with histone acetylases and deacetylases has been reported, functional interaction of Tax with histone methyltransferases (HMTase) has not been studied. Here we examined the ability of Tax to interact with a histone methyltransferase SUV39H1 and studied the functional effects of the interaction on HTLV-1 gene expression. We report that Tax interacts with SUV39H1 *in vitro*, and that a stronger binding is observed when mutant proteins retain the C-terminal half of SUV39H1 encompassing the SAC (SET-associated Cys-rich) and SET domains of SUV39H1 [30,31]. Our data indicate that Tax interaction does not affect the methytransferase activity of SUV39H1, but induces a relocalization of SUV39H1 in the nuclei resulting in colocalization with Tax. Furthermore, co-expression of SUV39H1 with N-terminal deletion mutant of Tax resulted in cytoplasmic distribution of both proteins. We further demonstrate that SUV39H1 represses Tax transactivation of HTLV-1 LTR promoter activity depending on the Suv39H1 methyltransferase activity and revealed induction of SUV39H1 expression by Tax and tethering of induced SUV39H1 to the HTLV-1 LTR. These data suggest a possible negative feedback loop of HTLV-1 gene expression in infected cells, which may be one of the bases for the induction of HTLV-1 latency.

Results

HTLV-1 Tax interacts with SUV39H1

To determine whether HTLV-1 Tax has the ability to interact with SUV39H1, we used GST pull-down and co-immunoprecipitation assays by transient transfection of

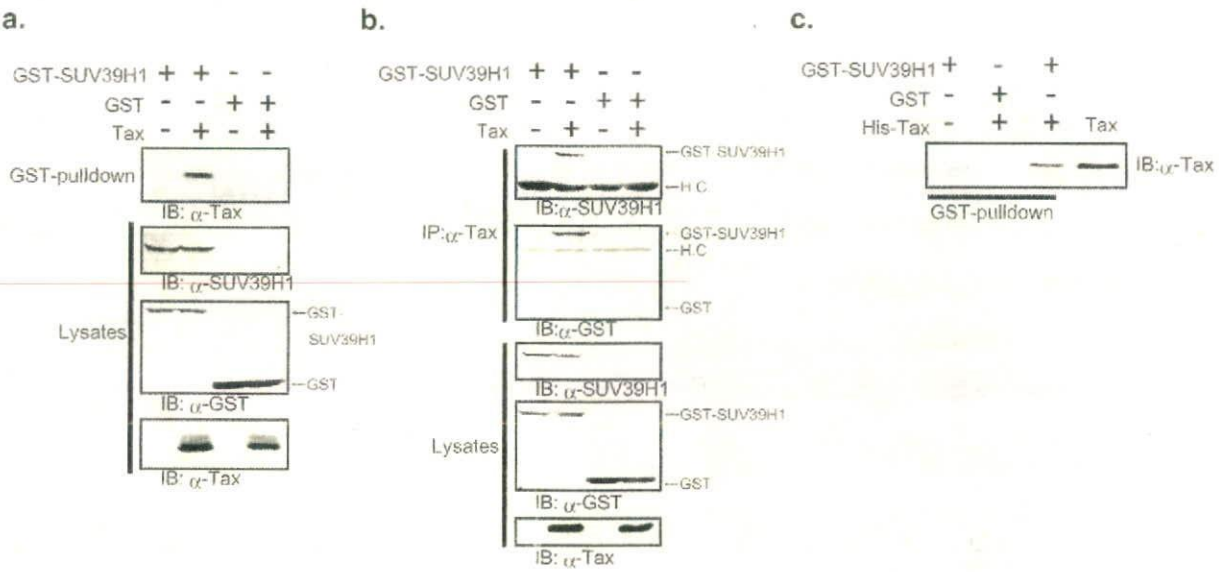

Figure 1

Tax interacts with SUV39H1 in vitro. (a) HEK293T cells were transiently cotransfected with GST-SUV39H1 or GST and Tax. After 48 h, the cells were lysed and the proteins were affinity purified with Glutathione Sepharose 4B. Purified proteins were separated by SDS-PAGE, transferred to a PVDF membrane, and probed with anti-Tax antibody Lt-4 (top panel). Expression of transduced proteins was confirmed by immunoblot analyses of whole cell lysates using respective antibodies (lower panels). (b) HEK293T cells were transiently co-transfected with expression plasmids, GST-SUV39H1 or GST and Tax. After 48 h, the cells were lysed and the proteins were immunoprecipitated with Lt-4. The immunoprecipitates were separated by SDS-PAGE, transferred to a PVDF membrane, and probed with anti-SUV39H1 or anti-GST antibody (upper panels). Expression of proteins was confirmed by immunoblot analyses of whole cell lysates using respective antibodies (lower panels). (c) Direct interaction between SUV39H1 and Tax. Bacterially expressed GST-SUV39H1 and GST were purified with Glutathione Sepharose 4B, and histidine-tagged wild type Tax (His-Tax) was purified with ProBond Resin (Promega). GST-SUV39H1 and GST were bound to Glutathione Sepharose 4B, and mixed with purified His-Tax in PBS. After centrifugation, proteins bound to Glutathione Sepharose 4B were separated by electrophoresis, transferred to a PVDF membrane, and probed with anti-Tax antibody. As a control, an aliquot of purified His-Tax was run in lane 4. IP, immunoprecipitation; IB, immunoblot; H.C., heavy chain

expression vectors for these proteins. Transient transduction was used for the experiments because the assays were not sufficiently sensitive with endogenous proteins and others also encountered this problem [32]. Expression vectors for the wild type HTLV-1 Tax (pCG-Tax) and GST-tagged SUV39H1 (pMEG-SUV39H1) were transfected into HEK293T cells as described in Materials and Methods. GST-SUV39H1 protein was affinity purified using Glutathione-Sepharose 4B column from total cellular proteins. Co-purified proteins were analyzed by immunoblotting using anti-Tax monoclonal antibody Lt-4 [33]. Total cellular proteins were also analyzed by immunoblotting as controls for protein expression using antibodies for SUV39H1, Tax and GST proteins. The results clearly showed that affinity-purified GST-SUV39H1 complex contained HTLV-1 Tax protein, whereas Tax protein was not co-purified with GST alone (Figure 1a). Conversely, when the cell lysates were immunoprecipitated with anti-Tax antibody Lt-4, the immune complex was shown to contain SUV39H1 that was detected by anti-SUV39H1 antibody as well as anti-GST antibody (Fig. 1b, upper two panels). Absence of Tax protein in the immune complex when GST protein alone was co-expressed denied the possibility that Tax might be co-immunoprecipitated because of the affinity to GST protein (Fig. 1b, lane 4). Taken together, these results suggested that wild type Tax interacts with SUV39H1 in cultured cells.

Next, we examined direct interaction between Tax and SUV39H1 using bacterially expressed and purified proteins. GST pull-down assays of histidine-tagged Tax and GST-fusion SUV39H1 were performed for this analysis.

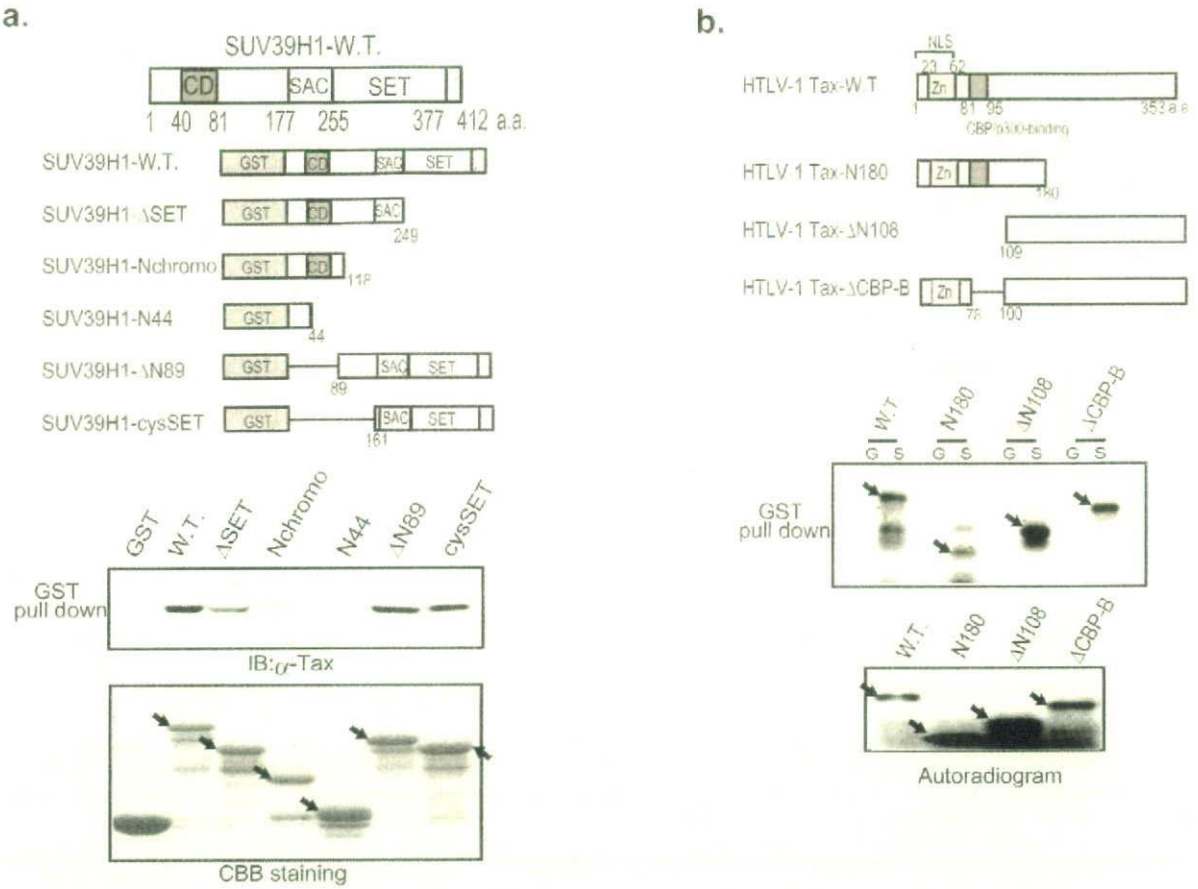

Figure 2

Analyses of the interacting domains. (a) GST pull-down assays using bacterially expressed GST-tagged wild type and various mutants of SUV39H1 and histidine-tagged wild type Tax (His-Tax). A schematic representation of the wild type (SUV39H1-WT) and those of domain structures of mutants are indicated in the upper panels. Results of the pull-down assays are shown in the lower panels. Pulled-down proteins were analyzed by SDS-PAGE and immunoblotting with Lt-4 antibody (top of the lower panels). The bottom panel shows the Coomassie Brilliant Blue (CBB)-stained gel where the wild type and various mutant SUV39H1 proteins were run. (b) Pull-down assays using the wild type GST-SUV39H1 and *in vitro* translated wild type and various mutant Tax proteins. Schematic description of the structures of wild type and various mutant Tax proteins is presented in the top panel. Results of the pull-down assays are shown in the top of the lower panels. Pulled-down Tax proteins that were labeled with ^{35}S-methionine were visualized by autoradiography (top of the lower panels). The bottom panel shows the autoradiogram of the gel where the radio labeled wild type and various mutant Tax proteins were run.

The results clearly showed that Tax protein directly interacts with GST-SUV39H1 but not with GST protein alone (Fig. 1c).

Binding domain analysis

To define the domains within SUV39H1 and Tax that are responsible for the interaction, we performed *in vitro* binding assays. First, we constructed various mutants of SUV39H1 according to the domain structure [34] (Fig. 2a, upper panel) and examined binding to the His-tagged wild type Tax protein that was bacterially expressed and purified by ProBond Resin (Promega). When C-terminally deleted series of SUV39H1 were examined, a mutant (ΔSET) that lost the SET domain and the C-terminal cysteine-rich region, but retained the SET-associated Cys-rich (SAC) domain, showed a significantly decreased binding (less than half of the band intensities of the wild type, ΔN108 and ΔCBP-B, when measured by NIH Image software). Further deletion up to amino acid 118 that resulted in loss of the SAC domain (a mutant named

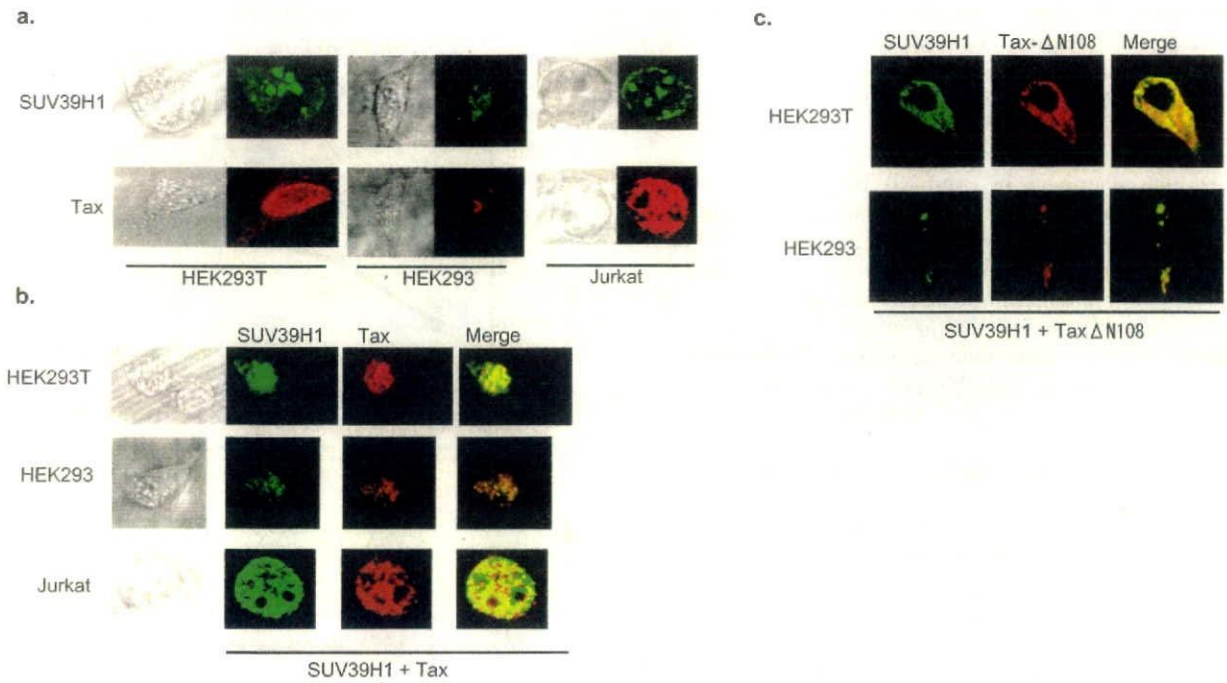

Figure 3
Immunofluorescence microscope analysis of SUV39H1 and Tax. (a) HEK293T, HEK293 and Jurkat cells were cultured on glass coverslips, transfected with SUV39H1 or Tax (upper and lower panels, respectively). Large and defined nuclear speckles were observed in the cells transfected with SUV39H1 (upper panels). Rather diffuse nuclear localization was observed in those transfected with Tax (lower panels). Phase contrast photographs are on the left of each immunofluorescence photograph. (b) HEK293T, HEK293 and Jurkat cells transfected with SUV39H1 and Tax expression plasmids together. Phase contrast photographs are on the left of immunofluorescence photographs. The merged photographs are shown on the right of each panel. (c) HEK293T and HEK293 cells transfected with SUV39H1 and TaxΔN108 together. The merged photograph is shown on the right.

Nchromo) showed very weak residual binding activity (about one tenth of the intensities of the wild type, ΔN108 and ΔCBP-B). A mutant retaining only the N-terminal 44 amino acids (N44) totally lost binding activity (Fig. 2a, top of the lower panels, lanes 2 to 5). Two N-terminally deleted mutants (ΔN89 and cycSET) were tested to narrow down the binding region. The ΔN89 mutant lacks the N-terminal region including the chromodomain but retains the region between the chromodomain and the SAC domain (amino acids 89 to 160). The cycSET mutant retains the SAC and SET domains with the C-terminal cysteine-rich region. GST pull-down assays showed that both mutants have strong binding activities, indicating that the loss of the amino acids from 89 to 160 does not affect binding activity. Taken together, although the interaction appears to be complex and may involve several domains, the region of amino acids from 161 to 412 (the SAC-SET domains and C-terminal cysteine-rich region) appears to be enough to show a high affinity for Tax protein. Since the defined region comprises the catalytic motif required for the HMTase activity [34], the results shown above indicate that the catalytic region of SUV39H1 appears to play an important role in the interaction with Tax.

We then analyzed the domains of Tax protein responsible for the interaction with SUV39H1. In addition to the wild type Tax, we used three kinds of mutants, TaxN180, TaxΔN108 and ΔCBP-B. TaxN180 has a C-terminal deletion up to 180 amino acids, TaxΔN108 a deletion of N-terminal 108 amino acids and ΔCBP-B a deletion of the CBP binding domain (amino acids from 79 to 99) (Fig. 2b, upper panel). After *in vitro* translation and labeling with ^{35}S-Methionine, the wild type Tax and these mutants were used for *in vitro* pull-down assays with GST-SUV39H1. The results demonstrated that the wild type Tax and all these mutants can bind to SUV39H1 (Fig. 2b, top of the lower panels). However, TaxN180 showed a significantly weaker binding compared with other proteins (about half of the radioactivity of the wild type Tax), suggesting that

the C-terminal region of Tax may have a higher affinity for SUV39H1. Furthermore, it was shown that the p300/CBP-binding domain is dispensable for the interaction with SUV39H1 (Fig. 2b, top of the lower panels).

Co-localization of Tax and SUV39H1 in vivo

Next, we examined by confocal immunofluorescence analysis whether the intracellular localization of SUV39H1 may be influenced by interaction with Tax. When SUV39H1 alone was transduced in HEK293T, HEK293 and Jurkat cell lines, it showed large and defined nuclear speckles as reported previously [32,35] (Fig. 3a, upper panel). It is known that Tax usually shows speckled nuclear distribution [36,37], whereas in another report it shows diffuse nuclear localization [38]. In our experiments using HEK293T and Jurkat cells, transduced Tax showed diffuse nuclear localization similar to the previous report [38]. (Fig. 3a, lower panel). However, when these two proteins were simultaneously transduced, SUV39H1 protein did not show the speckled distribution and was diffusely distributed within the nuclei and colocalized with transduced Tax in all these cell lines (Fig. 3b). Since the distribution of Tax protein did not appear to have changed in the cells where both proteins were co-expressed, the results suggest a tethering of SUV39H1 by Tax.

To examine the possible tethering of SUV39H1 by Tax, we transduced an N-terminally deleted mutant Tax protein (TaxΔN108) lacking the nuclear localization signal and the wild type SUV39H1 in HEK293T and HEK293 cell lines. Transduced TaxΔN108 showed a clear cytoplasmic distribution as expected (Fig. 3c). In the presence of TaxΔN108, co-expressed SUV39H1 showed a cytoplasmic distribution instead of the nuclear localization seen when expressed alone (Fig. 3c). These results provide supportive evidence for the idea that Tax influences the cellular localization of SUV39H1.

SUV39H1 methyltransferase activity is not affected by the interaction with Tax

When two proteins interact with each other, functional modulation is expected to take place. Thus, we first examined whether association with Tax may affect the HMTase activity of SUV39H1, using *in vitro* methyltransferase assays according to the method reported by Fuks et al. with slight modifications [39]. First, we measured methyltransferase activities of immunoprecipitated SUV39H1 alone that was transduced in HEK293T cells, and studied the time course of the activities (Fig 4a). SUV39H1 immunoprecipitates methylated the substrate H3 (Fig. 4a, top panel). The levels of methylation appeared to become saturated at 60 min and thereafter (Fig. 4a, middle panel). Thus, we performed the reaction for 30 min to examine the effects of Tax on SUV39H1 HMTase activities. When

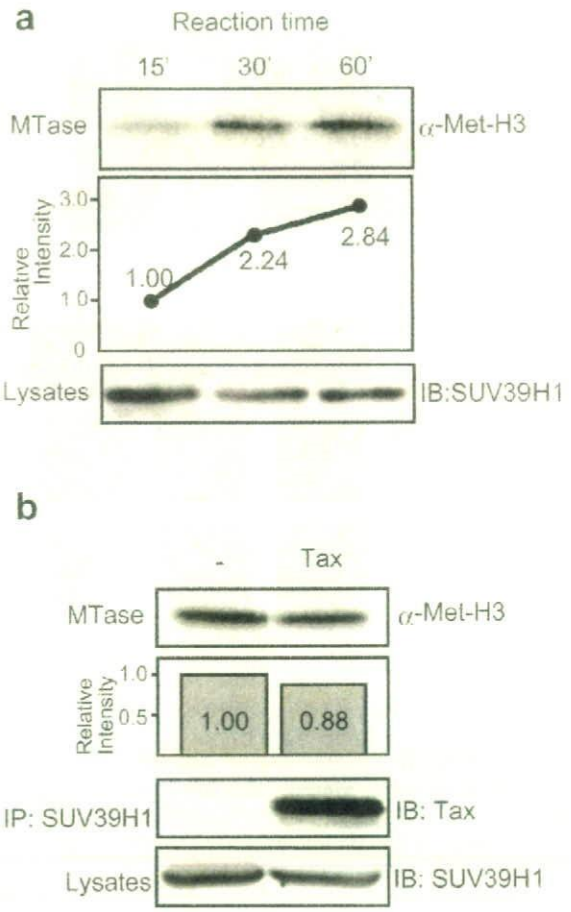

Figure 4

Results of *in vitro* methyltransferase assays. (a) Time course analysis. Top panel shows a representative fluorogram of the reaction mixtures at the indicated time points analyzed by 15% SDS-PAGE. The middle panel shows the relative levels of methylation measured by densitometric analyses of the bands. Bottom panel, a result of immunoblot analysis of transduced SUV39H1 by anti-SUV39H1 monoclonal antibody, showing comparable levels of SUV39H1 expression in each sample. (b) A representative result of three independent experiments of *in vitro* methyltransferase assays of SUV39H1 transduced with or without Tax. The reaction time was 30 min. The second panel shows the relative intensities of the methylated H3 bands. Lower panels show the results of immunoblot analyses of the immunoprecipitates and whole cell lysates to show the presence of SUV39H1 with or without Tax. IP, immunoprecipitation; IB, immunoblot. Antibodies used are indicated on the side of the panels.

Tax was co-expressed with SUV39H1 in HEK293T cells, the immunoprecipitates showed almost equal levels of methyltransferase activities compared with that of singly

expressed SUV39H1 (Fig. 4b, upper two panels). Taken together, these results suggest that although Tax shows a high affinity for the region containing the SET domain of SUV39H1, Tax does not affect the HMTase activity of SUV39H1 under the experimental condition used.

SUV39H1 represses Tax transactivation of HTLV-1 LTR promoter activity

Since Tax interacts with and tethers SUV39H1 without affecting HMTase activity, it is possible that SUV39H1 associated with Tax will methylate H3 K9 of the local chromatin where Tax is located, resulting in an interference of Tax function. One of the main biological functions of Tax is transcriptional transactivation of HTLV-1 LTR leading to efficient expression of viral RNA and viral replication in the infected cells. Thus, we examined the effects of SUV39H1 on transactivating function of Tax using pHTLV-LTR-Luc as a reporter. When transduced alone, Tax transactivated the HTLV-1 LTR promoter activity more than 200- and 20-fold in HEK293 and Jurkat cells, respectively. However, when SUV39H1 was co-transduced with Tax, the transactivation was dose-dependently suppressed in both cell lines down to the baseline levels with 500 ng or 1000 ng of the SUV39H1 plasmid (Fig. 5a, left and right panels). On the other hand, SUV39H1 alone showed only a little suppressive activity on the basal activities of HTLV-1 LTR promoter in both cell lines with corresponding amounts of the expression plasmid in the above experiments (Fig. 5b, left and right panels).

Next, we tested whether repression of Tax transactivation by SUV39H1 is dependent on the SUV39H1 methyltransferase activity. For this purpose, we used a loss-of-function mutant of SUV39H1 (H324L) reported by Lachner et al. [40], as well as deletion mutants used for the binding analysis. Co-expression of SUV39H1 (H324L) with Tax did not show a significant suppression of Tax transactivation of HTLV-1 LTR promoter activity (Fig. 5c). Furthermore, co-expression of C-terminal deletion mutants of SUV39H1 (ΔSET, Nchromo and N44) did not show any suppression of Tax transactivation, whereas co-expression of deletion mutants retaining the SAC-SET region (ΔN89 and cysSET) showed suppression of Tax transactivation similar to the levels by the wild type SUV39H1 (Fig. 5c).

Taken together, these results indicate that the interaction between SUV39H1 and Tax leads to repression of Tax transactivating function on HTLV-1 LTR depending on the HMT activity of SUV39H1.

Induction of SUV39H1 expression by Tax and localization on HTLV-1 LTR

Above results suggest that SUV39H1 may be a cellular protein counteracting with Tax function. Thus, we next tested the possibility that SUV39H1 expression may be induced by Tax, using JPX9 cells where Tax expression can be induced by $CdCl_2$ [41]. As was previously reported, treatment of JPX9 cells with $CdCl_2$ resulted in a strong induction of Tax, which was associated with SUV39H1 expression (Fig. 6a, upper figure, upper two panels). Since $CdCl_2$ treatment of Jurkat cells, from which JPX9 cells were derived, did not show any effects on the levels of SUV39H1 expression (Fig. 6a, lower figure), SUV39H1 appears to be induced by Tax as one of the Tax target genes.

Next, we examined whether Tax-induction of SUV39H1 leads to localization of SUV39H1 on the HTLV-1 LTR by chromatin immunoprecipitation (ChIP) assays using stable transformants of JPX9 cells transfected with the HTLV-1 LTR Luc plasmid (JPX9LTR clones). PCR analysis showed a clear difference between the ChIP samples of $CdCl_2$ treated (48 h) and untreated JPX9LTR clones (Fig. 6b, top panel). The intensity of the band was almost 10-fold stronger in $CdCl_2$ treated JPX9LTR cells than that of untreated cells measured by NIH Image software (Fig. 6b, second panel). The intensity of the PCR product from the $CdCl_2$ untreated JPX9LTR clones was almost the same as those from the samples of negative control without anti-SUV39H1 antibody (Fig. 6b). These results suggest that, with the induction of Tax expression, at least part of the induced SUV39H1 protein is recruited to the HTLV-1 LTR sequence. Detailed analyses of JPX9LTR clones as to time course of LTR promoter activities, protein expression levels, intracellular localization and so on are now under way in our laboratory, which will be reported in a separate paper.

To examine whether HTLV-1-infected cells express higher levels of SUV39H1, we studied SUV39H1 expression in T cell lines derived from ATL cells (TL-om1 and MT-1) as well as in those without HTLV-1 infection (Jurkat and CEM). The results clearly showed higher levels of SUV39H1 expression in ATL-derived T cell lines compared with T cell lines without HTLV-1 (Fig 6c, upper panel). These results suggest that SUV39H1 is one of the cellular target genes of Tax.

Discussion

Tax is a multi-functional regulatory protein encoded by HTLV-1. Through a protein-protein interaction, Tax deregulates multiple cellular processes including cell cycle progression, signal transduction and transcriptional regulation, which provide bases for HTLV-1 pathogenicity. In the present study, we demonstrated for the first time the interaction between HTLV-1 Tax and a histone methyltransferase SUV39H1. The interaction was largely dependent on the C-terminal half of the SUV39H1 protein that encompasses the SAC and SET domains and the

C-terminal cysteine-rich region. Interaction with Tax did not affect the SUV39H1 HMTase activity in *in vitro* methyltransferase assays. Tax tethered SUV39H1 resulting in colocalization with Tax in the nuclei and in the cytoplasm when an NLS (-) Tax mutant was expressed. These data provide strong supportive evidence for the idea that Tax directs the cellular localization of SUV39H1. Reporter gene assays showed that transduction of SUV39H1 represses Tax transactivation of HTLV-1 LTR promoter activity, which is dependent on the HMTase activity. Furthermore, endogenous SUV39H1 expression appeared to be induced by Tax expression in JPX9 cells, and induced SUV39H1 was shown to be recruited to the HTLV-1 LTR. Taken together, these data may suggest a negative feedback loop of HTLV-1 gene expression in the infected cells, where the transcriptional activator Tax itself may serve as a trigger for a self-limiting control over viral gene expression through the recruitment of SUV39H1 to HTLV-1 LTR and inducing H3 K9 methylation and a repressive histone code on the LTR.

By GST pull-down experiments, the Tax binding domain of SUV39H1 was narrowed down to the region covering the SAC and SET domains (Fig. 2a). On the other hand, the SUV39H1 binding domain of Tax was not clearly defined because all Tax mutants used showed affinities for SUV39H1 (Fig. 2b). However, the results indicated that the N-terminal region of about 100 amino acids of Tax is not essential for a high affinity interaction with SUV39H1 (Fig. 1b). This region contains the nuclear localization signal (NLS) and the CBP binding domain (CBP-B) [38,42]. The CBP-B of Tax does not appear to be involved in the binding to SUV39H1, since the amounts of the pull-down products of the mutants lacking this region (ΔCBP-B and TaxΔN108) were almost equal to that of the wild type (Fig. 2b), and co-expression of SUV39H1 with TaxΔN108 lacking NLS showed cytoplasmic localization of SUV39H1 (Fig. 3c). Many functional domains reside in the region where Tax shows a higher affinity for SUV39H1, such as those involved in the interaction with IKKγ [43], self-dimerization [44], and Rev-like nuclear export signal [45]. Thus, although SUV39H1 shares a functional characteristic with p300/CBP as histone modification enzymes, it appears to interact with Tax in a region distinct from that of p300/CBP. Consequently, the competition model proposed for repression of Tax transactivation by p53 may not be the mechanism by which SUV39H1 represses Tax transactivation.

Tax binding domain of SUV39H1 appears to be located in the C-terminal half region encompassing the SAC-SET and the C-terminal cysteine-rich regions (Fig. 2a). Our results contrast with previous reports showing that the N-terminal region of SUV39H1 is involved in the interaction with other proteins such as HP1b, HPC2, HDAC1 and 2 [31,32,46]. The interaction between SUV39H1 and the above proteins provides a scaffold for a functional multiprotein complex [39,47,48]. Furthermore, the N-terminal domain of 3–118 amino acids is considered the heterochromatin-targeting region. On the other hand, the SET domain is considered a dominant module which regulates SUV39H1 function such as chromatin distribution and protein interaction potentials [31]. The finding that interaction with Tax does not affect HMT activity of SUV39H1 (Fig. 4b) may suggest a new potential to form Tax-containing protein complexes in which above mentioned functions of SUV39H1 are preserved.

It was reported that endogenous SUV39H1 is a heterochromatic protein during interphase that selectively accumulates at centromeric positions of metaphase chromosomes [29,49]. Furthermore, the chromosomal localization of human SUV39H1 is very sensitive to protein expression levels [31]. In the present study, co-expression experiments showed a re-localization of nuclear SUV39H1, losing its typical speckled pattern in the presence of Tax (Fig. 3). SUV39H1 shows a rather diffuse distribution and co-localization with Tax in all cell lines used. These results suggest a possibility that Tax tethers SUV39H1 to the region where Tax is localized (Fig. 3b). This notion is supported by the observation that a mutant Tax lacking the NLS directs cytoplasmic localization of SUV39H1 (Fig. 3c). High levels of expression and coexistence of these proteins can be expected in the cells soon after HTLV-1 infection where the viral gene is vigorously transcribed and abundant Tax protein presumably coexists with high levels of SUV39H1 protein induced by Tax. If Tax tethers SUV39H1, Tax and SUV39H1 may form a repressive complex at the promoter where Tax is localized, thereby SUV39H1 may counteract the transcriptional activation by Tax. Our results of reporter gene assays and ChIP analysis showing dose-dependent repression of Tax transactivation of HTLV-1 LTR and SUV39H1 recruitment to the LTR after Tax induction in JPX9LTR cells provide a supportive evidence for this hypothesis. Thus, a negative feedback loop can be conceived by which HTLV-1 gene expression is made self-limiting. Since SUV39H1 can interact and form a complex with DNA methyltransferases [39], demonstration of SUV39H1 complex on HTLV-1 LTR may also provide a basis for the mechanism of heavy CpG methylation of HTLV-1 LTR in the latently infected cells in the peripheral blood and ATL cells *in vivo* [5].

Conclusion

In the present paper we demonstrated for the first time the interaction between SUV39H1 and HTLV-1 Tax, and apparent tethering of SUV39H1 by Tax, leading to co-localization in the nuclei. Since Tax interaction does not affect SUV39H1 HMTase activity, Tax-mediated tethering of SUV39H1 to the LTR and induction of a conforma-

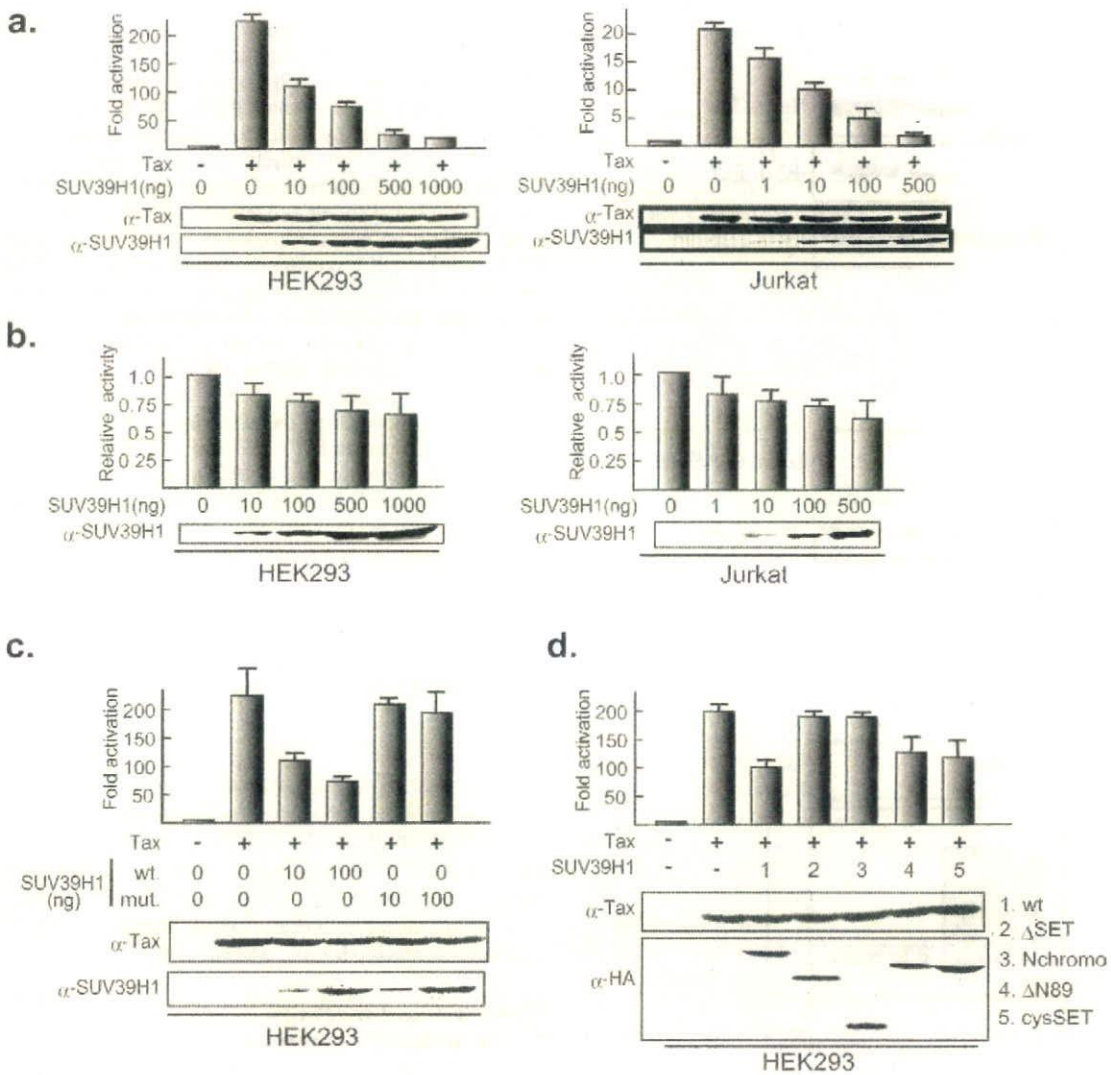

Figure 5

SUV39H1 represses Tax transactivation of HTLV-1 LTR promoter activity. Representative results of luciferase assays using HEK293 and Jurkat cells (left and right panels, respectively) are shown with the mean and standard deviation of triplicate experiments. Below the graphs, results of immunoblot analyses of whole cell lysates are shown to confirm expression of transduced proteins. (a) Dose-dependent repression of Tax transactivation of HTLV-1 LTR by SUV39H1. More than three independent assays were done for each cell line. (b) Effects of SUV39H1 on the basal activities of HTLV-1 LTR. In the absence of Tax, increasing amounts of SUV39H1 expression plasmid was transfected with HTLV-1 Luc. Left and right panels show the results of HEK293 and Jurkat cells, respectively. (c) Absence of repression of Tax transactivation by HMTase negative SUV39H1. Tax expression plasmid was co-transfected with the wild type or HMTase negative mutant SUV39H1 along with the reporter plasmid pHTLV LTR-Luc. Lower two panels show the results of immunoblot analyses to confirm the expression of transduced Tax and SUV39H1 proteins. Antibodies used are indicated on the left. (d) Suppressive activities of SUV39H1 mutants on Tax transactivation of HTLV-1 LTR promoter activity. Fold activation of HTLV LTR promoter activity by Tax is shown with the mean and standard deviation of triplicated experiments. Co-transfected HA-tagged mutant SUV39H1 constructs are indicated below the graph and on the right of lower panels. Structures of these deletion mutants are described in Fig. 2a, upper panel.

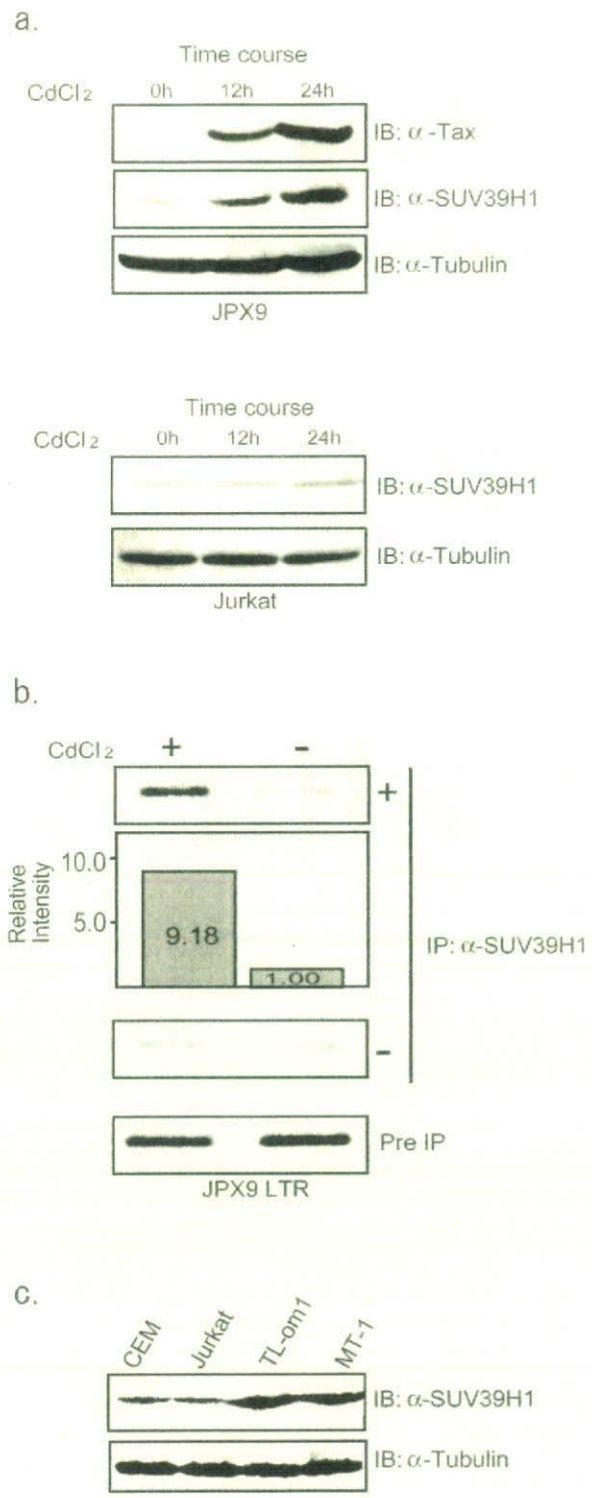

Figure 6
Induction of SUV39H1 expression in JPX9 cells and localization on the HTLV-1 LTR, and endogenous levels of SUV39H1 expression in T cell lines. (a) Top figure: Expression of Tax and SUV39H1 in $CdCl_2$-treated JPX9 cells. Whole cell lysates of JPX9 cells treated by $CdCl_2$ for indicated periods were studied by immunoblot analysis with anti-Tax and anti-SUV39H1 monoclonal antibodies (top and middle panels). The bottom panel shows the immunoblot by anti-tubulin antibody. Bottom figure: Absence of SUV39H1 induction in Jurkat cells by $CdCl_2$ treatment. Whole cell lysates of Jurkat cells treated by $CdCl_2$ for indicated periods were studied by immunoblot analysis with anti-SUV39H1 monoclonal antibody (top panel). The bottom panel shows the immunoblot by anti-tubulin antibody. (b) Results of ChIP assays. Representative photographs of agarose gel electrophoresis of PCR products are shown. Top panel shows results of $CdCl_2$-treated and untreated JPX9LTR clones. The relative intensities of the band measured by NIH Image software are shown in the second panel. The third and bottom panels show the results of negative controls without first antibody and input controls, respectively. (c) SUV39H1 expression in various T cell lines. ATL-derived cell lines (MT-1 and TL-om1) show higher levels of SUV39H1 expression compared with HTLV-1-uninfected cell lines (top panel). TL-om1 and MT-1 are ATL-derived and HTLV-1-infected cell lines. The bottom panel shows the immunoblot by anti-tubulin antibody.

tional change of the chromatin through H3 K9 methylation can explain the dose-dependent repression of Tax transactivation of LTR by SUV39H1. Taken together with the induction of endogenous SUV39H1 expression by Tax and the recruitment to the LTR, Tax-SUV39H1 interaction may form a negative feedback loop that self-limits HTLV-1 viral gene expression in infected cells

Materials and methods

Cell cultures and transfection

Jurkat, HEK293 and HEK293T cell lines were obtained from Fujisaki Cell Biology Center (Okayama, Japan) and the Japanese Cancer Research Resources Bank (Tokyo, Japan). JPX9, a cell line that can be induced to express Tax by $CdCl_2$ treatment, was a gift from Prof. Sugamura, Tohoku University. Jurkat and HEK293T cells were cultured in RPMI 1640 supplemented with 10% FCS and antibiotics, and in DMEM supplemented with 10% FCS and antibiotics, respectively. For the co-immunoprecipitation and *in vitro* methyltransferase assays, transfection was done by the standard calcium phosphate precipitation method using 8×10^5 HEK293T cells and a total of 30 μg of expression vectors. An empty expression vector pME18S or pMEG was used for control transfections or to make the total amount of transfected plasmid to be 30 μg.

Plasmids and cDNA

Human cDNA for SUV39H1 was amplified by RT-PCR from a normal human PBMC cDNA, and used after confirmation of the nucleotide sequence. The primers used for amplification were as follows: SUV39H1-F1: 5'-CCGCTCGAGATGGCGGAAAATTTAAAAGGCT-GCAGCGTG-3', SUV39H1-R1: 5'-GGACTAGTCTAGAA-GAGGTATTTGCGGCAGGACTCAGT-3'. GST-fusion proteins of mutants of SUV39H1 that lack functional domains were also prepared using PCR of the wild type cDNA. Forward primers: 5'-AAACTCGAGATGTTC-CACAAGGACTTAGAAAGGGAGCTG-3' (ΔN89), 5'-AAACTCGAGATGGTGTACATCAATGAGTACCGTGTT-GGT-3' (cysSET), Reverse primers, 5'-GGACTAGTGT-CATTGTAGGCAAACTTGTGCAGTGACGC-3' (wild type, ΔN89, cysSET), 5'-CCCACTAGTTCACCGGAAGATGCA-GAGGTCATATAGGAT-3' (ΔSET), 5'-CCCACTAGT-TCACAGGTAGTTGGCCAAGCTTGGGTCCAG-3' (Nchromo), 5'-CCCACTAGTTCACAGGTAGTT-GGCCAAGCTTGGGTCCAG-3' (N44). pGEX5X-3 (Amersham) was used to prepare bacterially expressed GST-fusion proteins. For the expression in mammalian cell lines, the following expression vectors were constructed. pMEG, a vector containing the humanized GST protein [50,51], was used to construct pMEG-SUV39H1, which was used for binding assays. pME-Flag-SUV39H1 was used for transient co-transfection and co-immunoprecipitation assays. For functional and immunohistochemical analyses, an expression vector pcDNA-HA-SUV39H1 was used. To prepare an expression vector for a kinase-negative SUV39H1, we mutated histidine codon 324 into a leucine codon according to Lachner et al [40] using PCR with a mutated primer. The region from nucleotide position 961 from ATG to 1239 (end of the stop codon) was amplified using a mutating forward primer (5'-TTTGT-CAACC*T*CAGTTGTGACCCCAACCTGCA-3') and a reverse primer SUV39H1-R1. The amplified fragment replaced the region of the wild type cDNA in pcDNA-HA-SUV39H1 using the HincII restriction enzyme site. The resultant plasmid has a mutated cDNA encoding leucine at 324 instead of histidine (H324L) and was named pcDNA-HA-SUV39H1-H324L. GST-fusion proteins were purified using Glutathione Sepharose 4B (Amersham), followed by confirmation with SDS-PAGE and CBB staining. For expression of histidine-tagged Tax protein, pET3d/Tax was prepared, and the fusion protein was purified by ProBond Resin (Invitrogen), followed by confirmation by SDS-PAGE and CBB staining.

in vitro *transcription and translation*

For *in vitro* translation of the wild type and mutant Tax proteins, the cDNA was amplified by PCR and cloned into pBluescript II SK (-). *in vitro* transcription and translation of the indicated cDNA was done using TNT QuickCoupled Transcription/Translation Systems (Promega). The proteins were labeled by incorporating ^{35}S-Methionine (Amersham), and confirmed by autoradiography of the SDS-PAGE of the products. The primers used are as follows: forward primer for wild type, N180 and ΔCBP-B, 5'-TGAATTCCATATGGCCCACTTCCCAGGGTTTGGA-3', forward primer for ΔN108, 5'-TGAATTCCATATGCG-CAAATACTCCCCCTTCCGA-3'; reverse primer for wild type, N180 and ΔCBP-B, 5'-AAACTCGAGGGATCCGACT-TCTGTTTCGCGGAAATGTTT-3', reverse primer for N180, 5'-CCCGAGCTGGCCGGGGTCGCAAAA-3'. A Tax mutant that lacks the CBP binding domain (amino acids 81 to 108) was prepared as follows. First, SpeI recognition site was introduced into the nucleotide positions of 238 to 243 and 334 to 339 by Kunkel's method, then the plasmid was digested by SpeI and the larger fragment was separated and recovered from agarose gel, followed by self-ligation. The oligonucleotides used for introduction of point mutations are as follows: MS-1: 5'-CTCCCCTCCT-TCCCCACTAGTAGAACCTCTAAGACC-3', MS-2 5'-CAGGCCATGCGCAAAACTAGTCCCTTCCGAAATGGA-3'.

GST pull-down assay

Wild type and mutant GST-SUV39H1 proteins (2 μg) bound to Glutathione-Sepharose 4B were mixed with His-tagged Tax protein (2 μg) in cold PBS and incubated at 4 °C for one hour. After centrifugation, proteins bound to Glutathione-Sepharose 4B were separated by 10% SDS-PAGE followed by immunoblot analysis using anti-Tax monoclonal antibody Lt-4. Relative intensities of the bands were determined using the NIH Image software. Binding analyses using *in vitro* translated and ^{35}S-labeled Tax proteins were done basically as described above. The amounts of *in vitro* translation products were one fourth of the reaction mixture. Binding was detected by autoradiography of the dried gel that had been fixed for 30 min in 10% acetic acid, 10% methanol, 10% glycerol followed by treatment with Amplify Fluorographic Reagent (Amersham) for 30 min. Relative intensities of signals were determined by Autoimage Analyzer (BAS2000, Fuji Photo Film, Tokyo).

Co-immunoprecipitation and immunoblotting

Immunoblots were done to detect co-immunoprecipitated or GST pull-down proteins, as described previously [52]. For co-immunoprecipitation analyses, cell lysates were prepared in TNE buffer (10 mM Tris-HCl, pH7.8, 1% Nonidet P-40, 150 mM NaCl, 1 mM EDTA). When indicated, aliquots were removed for immunoblots of whole cell lysates. Primary antibodies used were anti-SUV39H1 monoclonal antibody (abcam) and anti-Tax monoclonal antibody Lt-4 [33] and alkaline phosphatase-conjugated anti-mouse immunoglobulin sheep and anti-rabbit donkey antibodies (both from Promega) were used as secondary antibodies.

Immunohistochemistry

HEK293T cells (8×10^5) were grown on coverslips for one day, and transfected with 10 μg of pCG-Tax and 20 μg of pcDNA-HA-SUV39H1 by the calcium phosphate precipitation method. Jurkat cells (2×10^5) were transfected with 2 μg each of pCG-Tax and pcDNA-HA-SUV39H1 plasmids using Lipofectamine2000 (Invitrogen). After 36 hours, HEK293T cells were fixed with 4% paraformaldehyde for 10 min at room temperature, followed by permeabilization with 0.1% TritonX. Jurkat cells were harvested and fixed with acetone/methanol (1:1). Both cells were incubated with anti-Tax antibody Lt-4 and/or anti-HA antibody for one hour, followed by washing with PBS and incubation with fluorescence labeled secondary antibodies for one hour. The secondary antibodies used were Alexa Fluor 546 (anti-mouse antibody, Invitrogen) and Alexa Fluor 488 (anti-rabbit antibody, Invitrogen). Cells were fixed on a slide glass using mounting medium (PBS: glycerol, v:v = 1:9) and covered with a FluoroGuard antifade reagent (Bio-Rad). Fluorescence signals were detected using confocal microscopy (Radiance 2000, Bio-Rad).

in vitro *HMT assay*

The assay was done basically according to the method reported by Fuks et al. [39] with slight modifications. Briefly, SUV39H1 expression vector pME-Flag-SUV39H1 was transfected alone or with Tax expression vector pCG-Tax into HEK293T cells. After culturing for 40 hours, cells were lysed in TNE buffer, followed by immunoprecipitation with anti-FLAG M2 antibody. The immunoprecipitates were used for *in vitro* methyltransferase assay using histone octamer (Sigma) as substrates. Reaction was done at 30°C for indicated time in a reaction buffer containing 50 mM Tris-HCl, pH8.5, 20 mM KCl, 10 mM $MgCl_2$, 10 mM β-mercaptoethanol, and 250 mM sucrose) in the presence of 10 μCi ^{3}H-adenosylmethionine (Amersham). The reaction mixture was analyzed by 15% SDS-PAGE. After fixation, gels were treated with Amplify Fluorographic Reagent (Amersham) for 30 min and followed by fluorography. The levels of methylation were evaluated by densitometric analyses of the bands using NIH Image software.

Reporter Gene Assays

To study the transactivation of HTLV-1 LTR promoter by Tax, reporter gene assays were done, using pHTLV-LTR-Luc plasmid as a reporter and pCG-Tax as an effector in the presence or absence of SUV39H1. pHTLV-LTR-Luc and pCG-Tax were generous gifts from Prof. J Fujisawa, Kansai Medical University [53]. Briefly, a reporter plasmid, pHTLV-LTR-Luc, was constructed by inserting a 647-bp HTLV-1 LTR fragment into the MCS site of the pGL3 vector (Promega). HEK293 cells were transfected with 50 ng of pHTLV-LTR-Luc, 50 ng of pCG-Tax and 10 to 1,000 ng of pcDNA-HA-SUV39H1 by the calcium phosphate precipitation method. Jurkat cells were transfected with 100 ng of pHTLV-LTR-Luc, 10 ng of pCG-Tax and 10 to 500 ng of pcDNA-HA-SUV39H1 by the DEAE method [50]. A β-galactosidase expression plasmid driven by the β-actin promoter (pβ-act-β-gal) [54] was co-transfected to standardize each experiment. Cells were harvested 48 h after transfection, and Luciferase activity was measured with Luciferase assay kit (Promega). The measured activities were standardized by the activities of β-galactosidase, and transactivation was expressed as fold activation compared with the basal activity of LTR-Luc without effectors such as SUV39H1 or Tax. Representative results of triplicate experiments that were repeated more than three times are shown in the figures with the mean and standard deviation.

Induction of Tax expression in JPX9 cells

JPX9 cells were cultured in RPMI1640 supplemented with 10% FCS and antibiotics unless stimulated with $CdCl_2$. Tax expression in JPX9 cells was induced by culturing 1×10^6 cells in the presence of 30 μM $CdCl_2$ for indicated hours. Then, cells were harvested and lysed by 1 × sample buffer (65 mM Tris-HCl pH 6.8, 3% SDS, 10% glycerol, 0.01% BPB) followed by 10 min of boiling. Samples corresponding to 2×10^5 cells were separated by SDS-PAGE and transferred to PVDF membrane as described above. After blocking with skim milk, the membranes were incubated with the primary antibody at room temperature for one hour, washed in TBST buffer and incubated with the alkaline phosphatase-conjugated anti-mouse secondary antibody at room temperature for one hour. The primary antibodies used are as follows: anti-SUV39H1 mouse monoclonal antibody (abcam), anti-Tax mouse monoclonal antibody Lt-4, and anti-tubulin mouse monoclonal antibody (Santa Cruz).

Chromatin immunoprecipitation (ChIP) assays

To examine the tethering of SUV39H1 by Tax, we prepared JPX9 transformants that were stably transfected with the HTLV-1 LTR Luc plasmid and pA-puro plasmid. After cloning by limiting dilution, isolated clones were tested for induction of Tax expression and luciferase activities by $CdCl_2$ treatment, and selected clones were named JPX9LTR clones (Detailed analyses using these clones will be reported in a separate paper). Using three JPX9 LTR clones, ChIP assays were performed to test tethering of SUV39H1 to the HTLV-1 LTR after Tax expression. Cells (2×10^6 per clone) were treated with or without $CdCl_2$ for 48 hours followed by cross-linking at 37°C for 10 min with formaldehyde (1% final concentration). Cells were pelleted by centrifugation and resuspended in 1 ml of ice-cold PBS (-) with protease inhibitor cocktail (Sigma). Cells were again pelleted by centrifugation at 4°C. The pellet was suspended in 500 μl of the lysis buffer (1% SDS, 10 mM EDTA, 50 mM Tris-HCl [pH8.1]) and kept on

ice for 10 min. After sonication on ice with an Astrason Ultrasonic Processor (Misonix) to shear DNA to lengths of between 200 and 1,000 bp (as estimated by agarose gel electrophoresis), lysates were cleared by centrifugation. The supernatant was then diluted 10-fold with dilution buffer (0.01% SDS, 1.1% Triton, 1.2 mM EDTA, 16.7 mM Tris-HCl [pH 8.1], 16.7 mM NaCl) with protease inhibitors to a final volume of 5 ml. An aliquot (500 μl) of the supernatant was saved to represent unfractionated chromatin. The diluted cell supernatant was precleared with a 50% suspension of protein G Sepharose beads (Sigma) for 30 minutes at 4°C with agitation. Sepharose was pelleted by brief centrifugation and the supernatant was transferred to a new tube. The cross-linked chromatin suspension was mixed with anti-SUV39H1 antibody or PBS as negative controls, and incubated overnight at 4°C. Immune complexes were reacted for 1 h at 4°C with agitation with a 50% suspension of protein G-Sepharose beads equilibrated with dilution buffer. After the reaction, the beads were collected and washed serially with the following buffers: buffer a [0.1% SDS, 1% Triton X-100, 2 mM EDTA, 20 mM Tris-HCl[pH8.1], 150 mM NaCl], buffer b [0.1% SDS, 1% Triton X-100, 2 mM EDTA, 20 mM Tris-HCl[pH8.1], 500 mM NaCl], buffer c [0.25 M LiCl, 1% NP-40, 1% Sodium Deoxycholate, 1 mM EDTA, 10 mM Tris-HCl[pH8.1], and TE. Immune complexes were eluted twice with 250 μl of elution buffer (1% SDS, 0.1 M $NaHCO_3$) for 15 min at room temperature and 20 μl of 5 M NaCl was added to the 500 μl eluates. Cross-links were reversed by heating at 65°C for 4 h, followed by addition of 10 μl 0.5 M EDTA, 20 μl 1 M Tris-HCl [pH6.5], and incubated at 45°C for 1 h in the presence of 40 μg/ml of proteinase K. The DNA was purified by phenol/chloroform extraction followed by ethanol precipitation. The recovered DNA was resuspended in 50 μl of TE. PCR was performed in 50 μl with Ampli Taq (Perkin-Elmer) and for 35 cycles (annealing temperature is 55°C). The set of primers used was as follows; forward 5'-ACAGAAGTCTGAGAAGGTCA -3' and reverse 5'-TGGGTGGTTCCCGGTGGCTT -3'. The predicted PCR product length is 150 bp. All PCR signals stained with Ethidium Bromide on 2.0% agarose gel were quantified with the NIH Image software.

Competing interests

The author(s) declare that they have no competing interests.

Authors' contributions

KK carried out co-immunoprecipitation assays, confocal immunofluorescence analysis and reporter gene assays, and prepared the figures. KY participated in construction of mutant expression plasmids, and performed *in vitro* binding assays. Aya M participated in construction of a methyltransferase negative mutant of SUV39H1 performed a part of reporter gene assays. Ari M prepared JPK9 LTR clones and performed ChIP assays. TI participated in the experimental design and data analysis, and performed *in vitro* HMTase assays. YT provided anti-Tax monoclonal antibody Lt-4 and contributed to experimental design and data analysis. MM participated in the experimental design, data analysis and writing of the manuscript. TW conceived of the study, and participated in its design and coordination, and data analysis, as well as in writing the manuscript. All authors have read and approved the final manuscript.

Acknowledgements

We thank Prof. Jun-ichi Fujisawa for pCG-Tax and pHTLV-LTR-Luc plasmids, and Ms A. Hamano and Ms M. Maruyama-Nagai for helping our work. This work was supported by Grants-in-Aid for Scientific Research from Ministry of Education, Culture, Sports, Science and Technology of Japan to T. Ishida and T. Watanabe.

References

1. Poiesz BJ, Ruscetti FW, Gazdar AF, Bunn PA, Minna JD, Gallo RC: **Detection and isolation of type C retrovirus particles from fresh and cultured lymphocytes of a patient with cutaneous T-cell lymphoma.** *Proc Natl Acad Sci U S A* 1980, **77**:7415-7419.
2. Yoshida M, Miyoshi I, Hinuma Y: **Isolation and characterization of retrovirus from cell lines of human adult T-cell leukemia and its implication in the disease.** *Proc Natl Acad Sci U S A* 1982, **79**:2031-2035.
3. Yamaguchi K, Watanabe T: **Human T lymphotropic virus type-I and adult T-cell leukemia in Japan.** *Int J Hematol* 2002, **76 Suppl 2**:240-245.
4. Watanabe T: **HTLV-I-associated diseases.** *Int J Hematol* 1997, **66**:257-278.
5. Koiwa T, Hamano-Usami A, Ishida T, Okayama A, Yamaguchi K, Kamihira S, Watanabe T: **5'-long terminal repeat-selective CpG methylation of latent human T-cell leukemia virus type I provirus in vitro and in vivo.** *J Virol* 2002, **76**:9389-9397.
6. Hironaka N, Mochida K, Mori N, Maeda M, Yamamoto N, Yamaoka S: **Tax-independent constitutive IkappaB kinase activation in adult T-cell leukemia cells.** *Neoplasia* 2004, **6**:266-278.
7. Gatza ML, Watt JC, Marriott SJ: **Cellular transformation by the HTLV-I Tax protein, a jack-of-all-trades.** *Oncogene* 2003, **22**:5141-5149.
8. Yoshida M: **Multiple viral strategies of HTLV-I for dysregulation of cell growth control.** *Annu Rev Immunol* 2001, **19**:475-496.
9. Mesnard JM, Devaux C: **Multiple control levels of cell proliferation by human T-cell leukemia virus type I Tax protein.** *Virology* 1999, **257**:277-284.
10. Bex F, Gaynor RB: **Regulation of gene expression by HTLV-I Tax protein.** *Methods* 1998, **16**:83-94.
11. Suzuki T, Fujisawa JI, Toita M, Yoshida M: **The trans-activator tax of human T-cell leukemia virus type I (HTLV-1) interacts with cAMP-responsive element (CRE) binding and CRE modulator proteins that bind to the 21-base-pair enhancer of HTLV-1.** *Proc Natl Acad Sci U S A* 1993, **90**:610-614.
12. Zhao LJ, Giam CZ: **Human T-cell lymphotropic virus type I (HTLV-I) transcriptional activator, Tax, enhances CREB binding to HTLV-I 21-base-pair repeats by protein-protein interaction.** *Proc Natl Acad Sci U S A* 1992, **89**:7070-7074.
13. Bantignies F, Rousset R, Desbois C, Jalinot P: **Genetic characterization of transactivation of the human T-cell leukemia virus type I promoter: Binding of Tax to Tax-responsive element 1 is mediated by the cyclic AMP-responsive members of the CREB/ATF family of transcription factors.** *Mol Cell Biol* 1996, **16**:2174-2182.
14. Shnyreva M, Munder T: **The oncoprotein Tax of the human T-cell leukemia virus type I activates transcription via interaction with cellular ATF-1/CREB factors in Saccharomyces cerevisiae.** *J Virol* 1996, **70**:7478-7484.

15. Kwok RP, Laurance ME, Lundblad JR, Goldman PS, Shih H, Connor LM, Marriott SJ, Goodman RH: **Control of cAMP-regulated enhancers by the viral transactivator Tax through CREB and the co-activator CBP.** *Nature* 1996, **380**:642-646.
16. Riou P, Bex F, Gazzolo L: **The human T cell leukemia/lymphotropic virus type I Tax protein represses MyoD-dependent transcription by inhibiting MyoD-binding to the KIX domain of p300. A potential mechanism for Tax-mediated repression of the transcriptional activity of basic helix-loop-helix factors.** *J Biol Chem* 2000, **275**:10551-10560.
17. Vo N, Goodman RH: **CREB-binding protein and p300 in transcriptional regulation.** *J Biol Chem* 2001, **276**:13505-13508.
18. Fry CJ, Peterson CL: **Transcription. Unlocking the gates to gene expression.** *Science* 2002, **295**:1847-1848.
19. Pise-Masison CA, Mahieux R, Radonovich M, Jiang H, Brady JN: **Human T-lymphotropic virus type I Tax protein utilizes distinct pathways for p53 inhibition that are cell type-dependent.** *J Biol Chem* 2001, **276**:200-205.
20. Ego T, Ariumi Y, Shimotohno K: **The interaction of HTLV-I Tax with HDAC1 negatively regulates the viral gene expression.** *Oncogene* 2002, **21**:7241-7246.
21. Goll MG, Bestor TH: **Histone modification and replacement in chromatin activation.** *Genes Dev* 2002, **16**:1739-1742.
22. Zhang Y, Reinberg D: **Transcription regulation by histone methylation: interplay between different covalent modifications of the core histone tails.** *Genes Dev* 2001, **15**:2343-2360.
23. Jenuwein T, Allis CD: **Translating the histone code.** *Science* 2001, **293**:1074-1080.
24. Strahl BD, Allis CD: **The language of covalent histone modifications.** *Nature* 2000, **403**:41-45.
25. Turner BM: **Cellular memory and the histone code.** *Cell* 2002, **111**:285-291.
26. Litt MD, Simpson M, Gaszner M, Allis CD, Felsenfeld G: **Correlation between histone lysine methylation and developmental changes at the chicken beta-globin locus.** *Science* 2001, **293**:2453-2455.
27. Noma K, Allis CD, Grewal SI: **Transitions in distinct histone H3 methylation patterns at the heterochromatin domain boundaries.** *Science* 2001, **293**:1150-1155.
28. Tachibana M, Sugimoto K, Fukushima T, Shinkai Y: **Set domain-containing protein, G9a, is a novel lysine-preferring mammalian histone methyltransferase with hyperactivity and specific selectivity to lysines 9 and 27 of histone H3.** *J Biol Chem* 2001, **276**:25309-25317.
29. Aagaard L, Laible G, Selenko P, Schmid M, Dorn R, Schotta G, Kuhfittig S, Wolf A, Lebersorger A, Singh PB, Reuter G, Jenuwein T: **Functional mammalian homologues of the Drosophila PEV-modifier Su(var)3-9 encode centromere-associated proteins which complex with the heterochromatin component M31.** *Embo J* 1999, **18**:1923-1938.
30. Huang N, vom Baur E, Garnier JM, Lerouge T, Vonesch JL, Lutz Y, Chambon P, Losson R: **Two distinct nuclear receptor interaction domains in NSD1, a novel SET protein that exhibits characteristics of both corepressors and coactivators.** *Embo J* 1998, **17**:3398-3412.
31. Melcher M, Schmid M, Aagaard L, Selenko P, Laible G, Jenuwein T: **Structure-function analysis of SUV39H1 reveals a dominant role in heterochromatin organization, chromosome segregation, and mitotic progression.** *Mol Cell Biol* 2000, **20**:3728-3741.
32. Sewalt RG, Lachner M, Vargas M, Hamer KM, den Blaauwen JL, Hendrix T, Melcher M, Schweizer D, Jenuwein T, Otte AP: **Selective interactions between vertebrate polycomb homologs and the SUV39H1 histone lysine methyltransferase suggest that histone H3-K9 methylation contributes to chromosomal targeting of Polycomb group proteins.** *Mol Cell Biol* 2002, **22**:5539-5553.
33. Tanaka Y, Yoshida A, Takayama Y, Tsujimoto H, Tsujimoto A, Hayami M, Tozawa H: **Heterogeneity of antigen molecules recognized by anti-tax1 monoclonal antibody Lt-4 in cell lines bearing human T cell leukemia virus type I and related retroviruses.** *Jpn J Cancer Res* 1990, **81**:225-231.
34. Rea S, Eisenhaber F, O'Carroll D, Strahl BD, Sun ZW, Schmid M, Opravil S, Mechtler K, Ponting CP, Allis CD, Jenuwein T: **Regulation of chromatin structure by site-specific histone H3 methyltransferases.** *Nature* 2000, **406**:593-599.
35. Chakraborty S, Sinha KK, Senyuk V, Nucifora G: **SUV39H1 interacts with AML1 and abrogates AML1 transactivity. AML1 is methylated in vivo.** *Oncogene* 2003, **22**:5229-5237.
36. Bex F, McDowall A, Burny A, Gaynor R: **The human T-cell leukemia virus type I transactivator protein Tax colocalizes in unique nuclear structures with NF-kappaB proteins.** *J Virol* 1997, **71**:3484-3497.
37. Semmes OJ, Jeang KT: **Localization of human T-cell leukemia virus type I tax to subnuclear compartments that overlap with interchromatin speckles.** *J Virol* 1996, **70**:6347-6357.
38. Smith MR, Greene WC: **Characterization of a novel nuclear localization signal in the HTLV-I tax transactivator protein.** *Virology* 1992, **187**:316-320.
39. Fuks F, Hurd PJ, Deplus R, Kouzarides T: **The DNA methyltransferases associate with HP1 and the SUV39H1 histone methyltransferase.** *Nucleic Acids Res* 2003, **31**:2305-2312.
40. Lachner M, O'Carroll D, Rea S, Mechtler K, Jenuwein T: **Methylation of histone H3 lysine 9 creates a binding site for HP1 proteins.** *Nature* 2001, **410**:116-120.
41. Nagata K, Ohtani K, Nakamura M, Sugamura K: **Activation of endogenous c-fos proto-oncogene expression by human T-cell leukemia virus type I-encoded p40tax protein in the human T-cell line, Jurkat.** *J Virol* 1989, **63**:3220-3226.
42. Harrod R, Tang Y, Nicot C, Lu HS, Vassilev A, Nakatani Y, Giam CZ: **An exposed KID-like domain in human T-cell lymphotropic virus type 1 Tax is responsible for the recruitment of coactivators CBP/p300.** *Mol Cell Biol* 1998, **18**:5052-5061.
43. Chun AC, Zhou Y, Wong CM, Kung HF, Jeang KT, Jin DY: **Coiled-coil motif as a structural basis for the interaction of HTLV type I Tax with cellular cofactors.** *AIDS Res Hum Retroviruses* 2000, **16**:1689-1694.
44. Tie F, Adya N, Greene WC, Giam CZ: **Interaction of the human T-lymphotropic virus type I Tax dimer with CREB and the viral 21-base-pair repeat.** *J Virol* 1996, **70**:8368-8374.
45. Burton M, Upadhyaya CD, Maier B, Hope TJ, Semmes OJ: **Human T-cell leukemia virus type I Tax shuttles between functionally discrete subcellular targets.** *J Virol* 2000, **74**:2351-2364.
46. Vaute O, Nicolas E, Vandel L, Trouche D: **Functional and physical interaction between the histone methyl transferase Suv39H1 and histone deacetylases.** *Nucleic Acids Res* 2002, **30**:475-481.
47. Fujita N, Watanabe S, Ichimura T, Tsuruzoe S, Shinkai Y, Tachibana M, Chiba T, Nakao M: **Methyl-CpG binding domain 1 (MBD1) interacts with the Suv39h1-HP1 heterochromatic complex for DNA methylation-based transcriptional repression.** *J Biol Chem* 2003, **278**:24132-24138.
48. Vandel L, Nicolas E, Vaute O, Ferreira R, Ait-Si-Ali S, Trouche D: **Transcriptional repression by the retinoblastoma protein through the recruitment of a histone methyltransferase.** *Mol Cell Biol* 2001, **21**:6484-6494.
49. Aagaard L, Schmid M, Warburton P, Jenuwein T: **Mitotic phosphorylation of SUV39H1, a novel component of active centromeres, coincides with transient accumulation at mammalian centromeres.** *J Cell Sci* 2000, **113 (Pt 5)**:817-829.
50. Ishida T, Mizushima S, Azuma S, Kobayashi N, Tojo T, Suzuki K, Aizawa S, Watanabe T, Mosialos G, Kieff E, Yamamoto T, Inoue J: **Identification of TRAF6, a novel tumor necrosis factor receptor-associated factor protein that mediates signaling from an amino-terminal domain of the CD40 cytoplasmic region.** *J Biol Chem* 1996, **271**:28745-28748.
51. Ishida TK, Tojo T, Aoki T, Kobayashi N, Ohishi T, Watanabe T, Yamamoto T, Inoue J: **TRAF5, a novel tumor necrosis factor receptor-associated factor family protein, mediates CD40 signaling.** *Proc Natl Acad Sci U S A* 1996, **93**:9437-9442.
52. Horie R, Ito K, Tatewaki M, Nagai M, Aizawa S, Higashihara M, Ishida T, Inoue J, Takizawa H, Watanabe T: **A variant CD30 protein lacking extracellular and transmembrane domains is induced in HL-60 by tetradecanoylphorbol acetate and is expressed in alveolar macrophages.** *Blood* 1996, **88**:2422-2432.
53. Furuta RA, Sugiura K, Kawakita S, Inada T, Ikehara S, Matsuda T, Fujisawa J: **Mouse model for the equilibration interaction between the host immune system and human T-cell leukemia virus type I gene expression.** *J Virol* 2002, **76**:2703-2713.
54. Ishida T, Yamauchi K, Ishikawa K, Yamamoto T: **Molecular cloning and characterization of the promoter region of the human c-erbA alpha gene.** *Biochem Biophys Res Commun* 1993, **191**:831-839.

Leukemia (2006) 20, 800–806

www.nature.com/leu

ORIGINAL ARTICLE

DHMEQ, a new NF-κB inhibitor, induces apoptosis and enhances fludarabine effects on chronic lymphocytic leukemia cells

R Horie[1,2,6], M Watanabe[1,6], T Okamura[3], M Taira[1], M Shoda[2], T Motoji[3], A Utsunomiya[4], T Watanabe[2], M Higashihara[1] and K Umezawa[5]

[1]Department of Hematology, School of Medicine, Kitasato University, Sagamihara, Kanagawa, Japan; [2]Laboratory of Tumor Cell Biology, Department of Medical Genome Sciences, Graduate School of Frontier Sciences, The University of Tokyo, Minato-ku, Tokyo, Japan; [3]Department of Hematology, Tokyo Women's Medical University, Shinjyuku-Ku, Tokyo, Japan; [4]Department of Hematology, Imamura Branch Hospital, Kagoshima, Japan and [5]Department of Applied Chemistry, Faculty of Science and Technology, Keio University, Yokohama, Kanagawa, Japan

Chronic lymphocytic leukemia (CLL) is a low-grade lymphoid malignancy incurable with conventional modalities of chemotherapy. Strong and constitutive nuclear factor kappa B (NF-κB) activation is a characteristic of CLL cells. We examined the effects of a new NF-κB inhibitor, dehydroxymethylepoxyquinomicin (DHMEQ), on CLL cells. Dehydroxymethylepoxyquinomicin completely abrogated constitutive NF-κB activity and induced apoptosis of CLL cells. Apoptosis induced by DHMEQ was accompanied by downregulation of NF-κB-dependent antiapoptotic genes: c-IAP, Bfl-1, Bcl-X_L and c-FLIP. Dehydroxymethylepoxyquinomicin also inhibited NF-κB induced by CD40 and enhanced fludarabine-mediated apoptosis of CLL cells. Results of this study suggest that inhibition of constitutive and inducible NF-κB by DHMEQ in combination with fludarabine is a promising strategy for the treatment of CLL.
Leukemia (2006) **20**, 800–806. doi:10.1038/sj.leu.2404167; published online 9 March 2006
Keywords: CLL; NF-κB; apoptosis; DHMEQ; fludarabine

Introduction

Chronic lymphocytic leukemia (CLL) is a low-grade B-cell malignancy predominantly affecting adults over the age of 50 years. The disease course is variable but remains incurable despite development of nucleoside analogues such as fludarabine and 2-chlorodeoxyadenosine (cladribine).[1] Development of a new treatment option based on the biological basis of CLL cells is needed to improve the prognosis of CLL. Most chemotherapeutic agents target the process of DNA replication and division of cells, therefore are more effective in tumor cells having high proliferation activity. These agents are not well suited for the treatment of CLL that shows not proliferation but instead an accumulation of cells through resistance to apoptosis.[2]

Recently, treatment strategies to target molecules that support the maintenance and growth of the tumor cells have been pursued.[3] Molecular target therapy increases the specificity of the agent to tumor cells, thereby minimizes undesirable toxicity to normal cells and provides an opportunity to cure malignancies incurable by conventional chemotherapy.[4,5]

It is important for development of a new treatment strategy of CLL to clarify a common biological basis for deregulated apoptosis and to develop specific agents that target the required molecule(s). Despite the diversity in clinical manifestations of CLL, strong and constitutive nuclear factor kappa B (NF-κB) activity is reported to be a common characteristic of CLL cells.[6] NF-κB activation has been connected with control of apoptosis.[7,8] This background suggests that in CLL cells, constitutively active NF-κB antagonizes apoptotic pathways leading to inappropriate survival of tumor cells. Recent studies using antibody against CD40 ligand (CD40L), which inhibits CD40 signaling, and a proteasome inhibitor support this hypothesis.[6,9,10] If so, targeting the NF-κB pathway and inhibition of NF-κB activity is a logical strategy to treat CLL.

Dehydroxymethylepoxyquinomicin (DHMEQ) is a new NF-κB inhibitor that is a 5-dehydroxymethyl derivative of a novel compound epoxyquinomicin C.[11] We showed that DHMEQ inhibits nuclear translocation of NF-κB.[12]

In the present study, using a new NF-κB inhibitor DHMEQ, we present data that indicate that constitutive NF-κB activation supports survival of CLL cells by induction of antiapoptotic genes. Dehydroxymethylepoxyquinomicin inhibited NF-κB activity induced by CD40 and enhanced fludarabine-mediated apoptosis of CLL cells, suggesting that inhibition of constitutive and inducible NF-κB by DHMEQ in combination with fludarabine is a promising strategy for the future treatment of CLL.

Materials and methods

Patients

All patients ($n=15$) were previously diagnosed as having B-cell CLL according to established clinical and laboratory criteria.[13] Patients were either untreated ($n=7$) or had received cytoreductive chemotherapy before investigation ($n=8$). Relevant clinical and laboratory data of the patients are included in Table 1.

Separation procedures and culture

Peripheral blood mononuclear cells (PBMC) were isolated from heparinized blood samples obtained after informed consent using gradient centrifugation with Lymphoprep (AXIS SHIELD PoC AS, Oslo, Norway). Chronic lymphocytic leukemia cells were purified using a Dynal B-cell-negative isolation kit (Dynal Biotech, Oslo, Norway). This method produced more than 95% pure population of CLL cells expressing both CD19 and CD5 (mean 97.8%), as determined by flow cytometry using antibodies anti-CD19/FITC and anti-CD5/PE (Dako, Kyoto,

Correspondence: Dr R Horie, Department of Hematology, School of Medicine, Kitasato University, 1-15-1 Kitasato, Sagamihara, Kanagawa 228-8555, Japan.
E-mail: rhorie@med.kitasato-u.ac.jp
[6]These authors contributed equally to this work.
Received 20 August 2005; revised 27 January 2006; accepted 30 January 2006; published online 9 March 2006

Table 1 Clinical data of the patients studied

Case #	Age (years)	Sex	WBC	Hb	Plt	Stage (Binet/Rai)	Therapy
1	89	M	41.2	11.6	14.7	A/0	None
2	58	M	33.3	14.2	13.8	A/0	None
3	67	M	20.0	12.7	13.7	A/0	None
4	88	M	14.8	12.0	10.8	A/0	None
5	67	M	7.8	9.5	16.1	C/IV	Fludara+Pred
6	79	M	71.2	12.4	9.5	C/IV	None
7	57	M	53.5	11.8	16.1	A/II	Fludara
8	83	F	26.5	15.2	11.6	A/0	None
9	62	M	48.7	7.6	2.7	C/IV	Fludara
10	72	M	23.1	14.3	10.7	A/0	None
11	72	F	74.5	9.2	10.2	C/III	CVP
12	70	F	12.8	8.4	1.7	C/IV	Fludara
13	72	F	202.5	6.9	1.6	C/IV	Fludara
14	89	M	133.9	7.6	5.9	C/IV	Fludara
15	75	M	90.8	11.2	8.7	C/IV	Cyclo

Abbreviations: CVP, cyclophosphamide, vincristine, prednisolone; Cyclo, cyclophosphamide; Fludara, fludarabine; Hb, hemoglobin (g/dl); Plt, platelet count ($\times 10^4/\mu l$); WBC, white blood cell count ($\times 10^3/\mu l$).

Japan). We purified normal B cells using the same method, which produced more than 90% pure population of B cells (mean 92.7%), assessed by flow cytometry staining with anti-CD19/FITC antibody (Dako, Kyoto, Japan). Cells were cultured at 37 C with 5% CO_2 in RPMI 1640 supplemented with 20% fetal bovine serum and antibiotics.

Chemicals

Dehydroxymethylepoxyquinomicin is an NF-κB inhibitor that blocks nuclear translocation of NF-κB.[11,12] An active metabolite of fludarabine, 2-fluoroadenine-9-β-D-arabinofuranoside (F-ara-A), was purchased from Sigma (St Louis, MO, USA). Dehydroxymethylepoxyquinomicin and F-ara-A were dissolved with dimethylsulfoxide (DMSO) and used for experiments at indicated concentrations. Bisbenzimide H 33342 fluorochrome (Hoechst 33342) and caspase-3 inhibitor Z-Asp-Glu-Val-Asp-(DEVD)-FMK were purchased from Calbiochem (Bad Soden, Germany).

Electrophoretic mobility shift analysis

Electrophoretic mobility shift analysis (EMSA) was carried out according to the methods described previously.[14] Double-stranded oligonucleotide probes containing the mouse immunoglobulin-κ light-chain NF-κB consensus site were purchased from Promega (Madison, WI, USA). Antibodies used for supershift assays were as follows: NF-κB p50 (C-19) goat polyclonal antibody, NF-κB p65 (C-20) and RelB (C-19) rabbit polyclonal antibody and mouse monoclonal antibodies for c-Rel (B-6) and NF-κB p52 (C-5) (all from Santa Cruz Biotechnology Inc., Santa Cruz, CA, USA).

Cell viability assay

Effects of DHMEQ on cell viability were assayed by color reaction with 3-(4,5-dimethylthiazol-2-yl)-2,5-diphenyl tetrazolium bromide (MTT assay) as described previously.[15] After incubation with DHMEQ at the indicated concentrations and time points, 2×10^5 cells treated by MTT solution were measured by a microplate reader (Bio-Rad, Richmond, CA, USA) at a reference wavelength of 570 nm and test wavelength of 450 nm. The cell viability was expressed as a percentage of the DMSO-treated control samples.

Apoptosis and analysis of caspase activity

To quantify apoptosis, cells were labeled with FITC-conjugated Annexin V (BD Biosciences, Palo Alto, CA, USA) followed by flow cytometric analysis. For analysis of morphological changes of nuclei, cells were stained by 10 μM Hoechst 33342, and photographed through a UV filter. Detection of cleaved caspase 3 was performed by immunohistochemistry. Antibodies used in these experiments were as follows: rabbit polyclonal antibody for cleaved caspase 3 (Asp175) (Cell Signaling, Beverly, MA, USA) and for glyceraldehyde phosphate dehydrogenase (FL335) (Santa Cruz Biotechnology Inc.). Mouse monoclonal antibody for Fas (CH-11) (Medical and Biological Laboratories Co., Ltd, Nagoya, Japan) was used for stimulation of Fas.

Real-time PCR analysis

Total RNA from isolated CLL cells was extracted using ISOGEN (Nippon Gene Co., Tokyo, Japan) according to the manufacturer's instructions. Single-stranded cDNA was synthesized using TaqMan Reverse Transcription Reagents (Applied Biosystems, Norwalk, CT, USA). The primers for Bcl-X_L; Hs00236329_m1 (BCL2L1) c-IAP; Hs00154109_m1 (BIRC3), Bfl-1; Hs00187845_m1 (BCL2A1) and c-FLIP; Hs00153439_m1 (CFLAR) were purchased from Applied Biosystems (Tokyo, Japan). The conditions of real-time PCR were as follows: 1 μl of cDNA was added to 25 μl of TaqMan Gene Expression Assays and made up to a total volume of 50 μl with distilled water for each reaction. Thermal cycler conditions were 2 min at 50 C, 10 min at 95 C and then 40 cycles of 15 s at 95 C followed by 1 min at 60 C. Results were collected and analyzed using an ABI PRISM 7000 sequence detection system (Applied Biosystems).

Statistical analysis

Differences between mean values were assessed by two-tailed *t*-test. A *P*-value <0.05 was considered to be statistically significant.

Results

Effects of DHMEQ on constitutive NF-κB activity in primary CLL cells

First we examined the effect of DHMEQ on constitutive NF-κB activity and its time course in CLL cells ($n=5$; #1, 2, 6, 7 and 14) by EMSA. As described previously, high NF-κB DNA binding activity was detected in nuclear extracts from CLL cells.[16] Treatment with 10 μg/ml of DHMEQ almost completely abrogated NF-κB DNA binding activity within 2 h. DNA binding activity of untreated CLL cells served as controls. Representative results (#7 and 14) are shown in Figure 1a. Supershift analysis of CLL cells ($n=5$; #1, 2, 6, 7 and 15) showed that NF-κB DNA binding activity consists of p50 homodimer (lower band) and p50/p65 heterodimer (upper band). Representative results (#2 and 15) are shown in Figure 1b. We next examined the effect of DHMEQ on constitutive NF-κB activity in all CLL cases studied ($n=15$). Treatment with 10 μg/ml of DHMEQ completely blocked NF-κB DNA binding activity in all cases. The results of 10 cases are shown in Figure 1c.